UCSF
UC San Francisco Electronic Theses and Dissertations

Title
Identifying differential effects of Parkinson's disease-causing mutations on LRRK2 cellular localization and substrate phosphorylation

Permalink
https://escholarship.org/uc/item/45p0j7k6

Author
Rinaldi, Capria

Publication Date
2023

Peer reviewed|Thesis/dissertation

eScholarship.org Powered by the California Digital Library
University of California

Identifying differential effects of Parkinson's disease-causing mutations on LRRK2 cellular localization and substrate phosphorylation

by
Capria Rinaldi

DISSERTATION
Submitted in partial satisfaction of the requirements for degree of
DOCTOR OF PHILOSOPHY

in

Pharmaceutical Sciences and Pharmacogenomics

in the

GRADUATE DIVISION
of the
UNIVERSITY OF CALIFORNIA, SAN FRANCISCO

Approved:

DocuSigned by:
Mark von Zastrow
2453D8468F7C43C...
Mark von Zastrow
Chair

DocuSigned by:
Kevan Shokat
Kevan Shokat

DocuSigned by:
Steven Altschuler
Steven Altschuler

DocuSigned by:
Lani Wu
6F84CA582ABA4BF...
Lani Wu

Committee Members

Acknowledgements

I am tremendously grateful to each and every person who has shaped my experience and cheered me on towards completing this dissertation.

Thank you to my graduate advisors, Steven Altschuler and Lani Wu. I am so grateful for the constant support you have given to me as your graduate student. Thank you for encouraging me to develop a thesis project from end-to-end. Though incredibly challenging scientifically and mentally, it was a truly rewarding experience. Thank you for giving me the freedom to make critical choices on my own but never letting me get too far off track. Thank you for providing an environment in which I felt comfortable sharing any issues or worries (so many worries!) that I had along the way. There was never a problem I faced that was too small for you to immediately help me come up with a plan or solution. You always had confidence in my work and my capability as a scientist, even when I doubted those things myself.

Thank you to those who played a role in my path to UCSF. To Joshua LaBaer, a fellow UCSF graduate, for giving me my first research experience in your group at the ASU Biodesign Institute and for allowing me to participate in your graduate seminar course as a college student. I will never forget this introduction to the scientific community. To Femina Rauf, my first research mentor, for your gentle, yet effective training style. I used the skills you taught me every day during my PhD. To Ana Carneiro at Vanderbilt University for an exciting summer research experience that exposed me to both neuroscience and quantitative microscopy – two interests I made sure to incorporate into my thesis work.

Thank you to the numerous scientific leaders at and around UCSF from whom I have had the privilege of receiving mentorship. To the members of my qualifying exam and thesis committees: Mark von Zastrow, Kevan Shokat, Sandra Schmid, Aimee Kao, Aparna Lakkaraju, and Jason Gestwicki, for your scientific expertise, your guidance, and your kindness. Thank you for encouraging me at every meeting, for helping me to structure an impactful research project,

and for reminding me to take a step back and enjoy the scientific process. To Su Guo, my first rotation advisor, for your instrumental role in my successful NSF GRFP application in my first year. Receiving this fellowship gave me scientific flexibility and more importantly, gave me confidence in myself early on in my graduate career. To Matt Jacobson, for believing in me from the beginning and for providing your scientific perspective at every step. Your excitement for my research findings and our literature discussions helped fuel my own interest in my thesis topic.

Thank you to the entire Altschuler-Wu lab, past and present; I am lucky to have found such an intelligent and kind group to work with. To Maike Roth, for introducing me to the lab during my rotation. To Louise Heinrich and Leanna Morinishi, for recruiting me to the original PhenoTIP team and for teaching me how to structure successful experiments. To Chris Waters, for your role in my project, for always being available for scientific advice, and for commiserating with me when things were hard. To my other co-authors, Zizheng Li, Lee Rao, and Karl Kumbier, for your contributions throughout my project. To Jake Bieber, for your friendship throughout the highs and lows; it was a privilege to have shared this experience with you. Thank you for always pulling your chair over to my desk, for taking lunch with me even if you had already eaten, and most importantly for teaching me that not everything is worth the stress.

Thank you to each of my friends, who have been there for me over the years. To my exceptionally talented PSPG classmates, for providing community and emotional support. Specifically, to Tia Tummino and Megan Koleske, for being unwavering cheerleaders, for encouraging me during the toughest periods, and for all of the memories we have shared inside and outside of our PhDs. You are two of the most caring and thoughtful people I have ever met. To my friends outside of UCSF near and far, Bianca Vora, Jenny Stokes, Logan Hille, Trisha Chaudhury, Nicholas Johnson, Marina Gunn Martin, and Bella Gunn, for always building me up and for giving me many opportunities to disconnect from grad school.

Thank you to my family, a never-ending source of encouragement. To my mom, Mini, for teaching me perseverance and independence, for always being available to talk, and for remembering to ask about every meeting or presentation I ever had. To my dad, Steve, for teaching me generosity and compassion, for making me feel like a superstar, and for always doing what you can to make my life easier and better. To my brother, Brady, for being my first best friend and for being someone I'm proud to have looked up to for my entire life. So much of who I am is because of you three. To Neale and little Rita, for being constant supporters and a bright light each time we FaceTime or visit. To each of my grandparents for your love and interest in my life. In particular, to my grandfather, Dr. Virendra Gupta, for being the first academic I knew and for inspiring me to follow a similar path. To all of the Goulders, especially Suzanne, for celebrating me at every milestone, no matter how small it felt to me. To Jenna and Nate, for bringing a piece of the family to San Francisco; we love getting to spend so much time with you. You have all made me feel like a part of your family for many years now.

Thank you, most of all, to my love and my best friend, Gregory Goulder. It is impossible to fully describe how much your love and support means to me. You have seen every part of this journey, and you have done so many things, big and small, to make each of my days brighter. I am grateful for every dinner you cooked for me, for every cute photo of Sage you sent to me, for every silly thing you did to make me laugh, and especially for every hug you gave me when things felt like too much. Through everything, you encouraged me to keep going because you believed in me, and for that I cannot thank you enough. I would not have finished this without you. I am lucky to spend my days with you, and I look forward to everything that comes next.

Contributions

Chapter 2:

Rinaldi, C., Waters, C.S., Li, Z., Kumbier, K., Rao, L., Nichols, R.J., Jacobson, M.P., Wu, L.F., and Altschuler, S.J. (2023). Dissecting the effects of GTPase and kinase domain mutations on LRRK2 endosomal localization and activity. Cell Reports. doi: 10.1016/j.celrep.2023.112447

Identifying differential effects of Parkinson's disease-causing mutations on LRRK2 cellular localization and substrate phosphorylation

Capria Rinaldi

Abstract

Mutations in the gene encoding leucine-rich repeat kinase 2 (LRRK2) are the most common known cause for Parkinson's disease (PD) and are associated with several other diseases, including cancer and autoimmune disease. Excitingly, several strategies to modulate LRRK2 activity in the brain are currently being tested in clinical trials for PD. Yet, there remain many unanswered questions as to how LRRK2 mutations affect cellular homeostasis and ultimately cause disease. Increasing our understanding of the cellular biology surrounding LRRK2 function is certain to aid in the acceleration of drug discovery and development in PD.

In Chapter 1, I broadly summarize the role of LRRK2 in PD and reported LRRK2 molecular and cellular functions. In particular, I describe the unanswered question of how PD-causing mutations in the kinase and GTPase domains of LRRK2 differentially affect observed LRRK2 kinase activity in cells. In Chapter 2, I present my published work detailing distinct cellular effects of PD-causing mutations in either the GTPase or kinase domain of LRRK2. Specifically, I found that GTPase-inactivating mutations strongly increase LRRK2 localization to endosomes upon inhibition of endosomal maturation. Under the same conditions, kinase-activating mutations only modestly affect LRRK2 localization and wild-type LRRK2 localization is minimally affected. I further demonstrate that the extent of LRRK2 endosomal localization is directly related to observed levels of LRRK2 substrate phosphorylation. Through this work, I provide a rationale for why PD-causing mutations across LRRK2 domains lead to differing levels of substrate phosphorylation in cells. Overall, my work highlights the importance of LRRK2's GTPase domain for the protein's cellular localization and activity and suggests that therapeutic strategies targeting LRRK2 GTPase function or localization may be beneficial for PD.

Table of Contents

List of Figures

List of Tables

List of Abbreviations

ASO: antisense oligonucleotide

DMSO: dimethyl sulfoxide

GFP: green fluorescent protein

GTP: guanosine triphosphate

LRRK2: leucine-rich repeat kinase 2

MEF: mouse embryonic fibroblast

PD: Parkinson's disease

SDM: site-directed mutagenesis

WB: Western blot

WT: wild-type

Chapter 1:

Introduction

1.1 Overview

Parkinson's disease (PD) is the second most common neurodegenerative disorder after Alzheimer's disease. PD affects approximately 1 million individuals in the United States and up to 10 million individuals around the world.[1,2] The lifetime risk for PD is around 2%, and the majority of patients are over the age of 60.[2] While over 20 genes (including SNCA, PRKN, PINK1, and LRRK2) have been determined to be causal for PD, only 10-15% of total PD cases are inherited from family members (familial PD).[3,4] The remaining 85-90% of cases are considered idiopathic or sporadic, with often unclear cause or genetic underpinnings.[5] Thus, in addition to genetics, age and environmental factors play an important role in developing PD.[4]

Clinically, PD is characterized by the progressive loss of dopaminergic neurons in the substantia nigra and the presence of Lewy bodies, which are aberrant neuronal inclusions largely composed of the α-synuclein protein and lipid membrane fragments.[6,7] Symptoms of PD, resulting from the loss of neurons in the central and peripheral nervous systems, are classified as both motor and nonmotor.[1,6] Motor symptoms often include movement and physical challenges such as tremor, stiffness, imbalance, and slowness, while nonmotor symptoms can include gastrointestinal issues, olfactory loss, sleep dysfunction, psychiatric disturbances, and cognitive impairment.[6]

A number of strategies exist to alleviate the motor and nonmotor symptoms of PD. Treatments for motor symptoms primarily include agents that increase or substitute for dopamine in the brain. Dopamine itself is unable to enter the brain. On the other hand, levodopa, which is the precursor of dopamine, can cross the blood-brain barrier and be metabolized to dopamine within the brain. Levodopa was first discovered to improve motor symptoms in the 1960s and is still the main therapeutic option for motor symptoms in PD patients.[1] In addition to levodopa, dopamine agonists and monoamine oxidase-B (MAO-B) inhibitors can be used to increase dopamine levels. Non-pharmacological therapies are

sometimes utilized for motor symptoms including deep brain stimulation and MRI-guided focused ultrasound.[6] Therapies for nonmotor symptoms are often the same as treatments used within the general population, including cholinesterase inhibitors, selective serotonin reuptake inhibitors (SSRIs), and tricyclic antidepressants.[6] While advances have been made in symptom management for PD, there are still no treatments approved for PD at this time that cure or modify the progression of the disease.

Despite the current lack of disease-modifying treatments for PD, drug discovery efforts to slow or reverse disease progression are ongoing and are often informed by the genetic causes of PD. In particular, targeting leucine-rich repeat kinase 2 (LRRK2) to slow PD progression has become the focus of several clinical-stage drug discovery efforts in recent years.[8]

1.2 LRRK2 Background

Mutations in the LRRK2 gene are the most common known genetic cause of PD, with the most frequent Gly2019Ser (G2019S) pathogenic mutation accounting for up to 5% of all familial and 1-2% of idiopathic PD cases.[8,9] Intriguingly, clinical features typically associated with LRRK2-PD have been described as indistinguishable from those observed in patients with idiopathic PD, including age of onset and neurodegeneration patterns.[2,8,10] Furthermore, increased LRRK2 kinase activity (a consequence of all disease-causing LRRK2 mutations) has also been described in dopaminergic neurons and microglia from patients with idiopathic PD.[5] These findings suggest that therapies targeting LRRK2 may also benefit the larger disease population and have further increased attention on LRRK2 as a promising drug target in PD.

The PARK8 chromosomal region containing the LRRK2 gene and later the gene itself were identified in the early 2000s through genetic analysis of a Japanese family in which 5 generations had individuals afflicted with autosomal dominant PD.[9,11–13] Since its discovery,

many studies have been dedicated to defining the LRRK2 structure, cellular function, and role in disease.

LRRK2 itself is a large, 2527 amino acid protein containing multiple protein domains, including protein-protein interaction domains and a catalytic core (**Figure 1.1**). The four protein-protein interaction domains include the N-terminal armadillo (ARM), ankyrin (ANK), and leucine-rich repeat (LRR) domains as well as the C-terminal WD40 domain. The catalytic core is comprised of a serine-threonine kinase domain and a Roc–COR tandem GTPase domain.[2,10] The kinase domain of LRRK2 is capable of phosphorylating residues within the protein itself as well as phosphorylating downstream protein substrates.[14] The function of the GTPase domain is less well-studied, though the protein's GTPase cycle is proposed to control kinase activity by influencing the conformational state, dimerization, and localization of LRRK2.[10,14,15] Accordingly, LRRK2 exists within cells in both monomers and dimers, with recent work describing an active tetramer LRRK2 complex.[2,16] LRRK2 monomers are typically cytosolic, while higher-order structures such as dimers are often membrane bound and are observed to have higher kinase activity.[2,15] At the tissue level, LRRK2 is widely expressed throughout the body, with the highest expression levels in the kidney, lung, and white blood cells in the peripheral immune system.[17] LRRK2 expression in the brain is relatively modest but can be detected in both neurons and glial cells.[18]

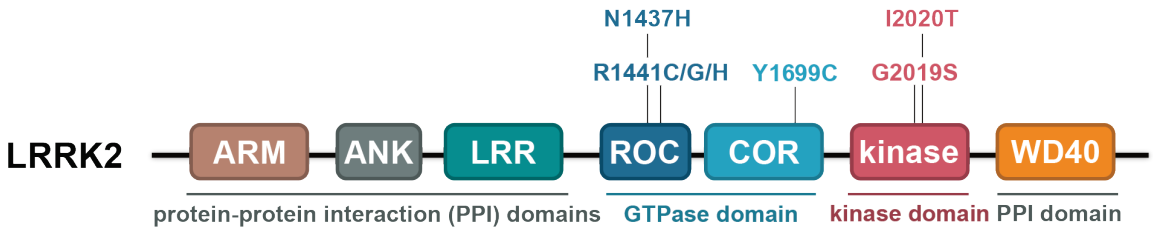

Figure 1.1: Domain structure of LRRK2. LRRK2 domain structure highlighting the seven Parkinson's disease-causing LRRK2 mutations, which all fall within the Roc-COR GTPase and kinase domains. ARM: Armadillo, ANK: Ankyrin, LRR: Leucine-rich repeat, ROC: Ras of complex, COR: C-terminal of ROC.

The importance of both the kinase and GTPase domains of LRRK2 is exemplified by the fact that all PD-causing mutations in LRRK2 are concentrated within these two domains. Specifically, two mutations in the kinase domain (G2019S and I2020T) and five mutations in the GTPase domain (N1437H, R1441C, R1441G, R1441H, and Y1699C) are considered causal for PD[9] (**Figure 1.1**). The G2019S mutation in the kinase domain is the most common, while the other mutations are relatively rare. Additional mutations exist within LRRK2 that are associated with increased risk for PD, including the G2385R mutation in the WD40 domain.[9] All disease-causing mutations in LRRK2 increase the phosphorylation of cellular substrates, albeit to differing degrees. In particular, the GTPase domain R1441C/G/H mutations increase cellular substrate phosphorylation levels to a significantly higher degree than the kinase domain G2019S mutation.[19,20] However, the mechanism behind this differential cellular activity is still unclear. Intriguingly, R1441C/G mutations are also reported to have a higher disease penetrance (>80%) than G2019S mutations (25-42.5%), suggesting a potential correlation between the degree of substrate phosphorylation and disease penetrance.[21–23]

Though it is clear that LRRK2 plays a prominent role in PD, the cellular functions of this protein remain incompletely defined. Described roles for LRRK2 since its discovery span multiple pathways and functions within the cell, including vesicular trafficking, cytoskeleton dynamics, autophagy, neurotransmission, lysosomal function, mitochondrial function, and others.[8] In 2016 and 2017, a subset of Rab GTPase (Rab) proteins were identified as LRRK2 phosphorylation substrates through phosphoproteomic screening[24,25] (**Figure 1.2**). Since this discovery, many efforts have focused on delineating downstream cellular consequences of Rab hyperphosphorylation by pathogenic LRRK2 mutants. Rab proteins are “master regulators of membrane trafficking” and function within intracellular trafficking pathways such as endocytosis, ER-Golgi trafficking, and autophagic flux.[26,27] Numerous studies have demonstrated that LRRK2 can be recruited to intracellular membranes (such as lysosomal or Golgi membranes) and

phosphorylate Rab proteins there, often in response to particular cellular stressors or environments.[28–35] Recent studies have identified functional roles for LRRK2-mediated Rab phosphorylation in ciliogenesis, regulating lysosomal damage, and mediating endosome-to-Golgi transport.[28] Still, the Rabs phosphorylated by LRRK2 have broad functions throughout multiple endo-lysosomal trafficking pathways[27,36] (**Figure 1.2**). Furthermore, many additional LRRK2 phosphorylation substrates have been suggested and await independent validation.[9] Finally, it is likely that LRRK2 is involved in multiple cellular processes given the wide range of LRRK2 phosphorylation substrates, expression throughout multiple tissues, and connection to multiple diseases.[37] Overall, there is more work to be done towards elucidating the relevant contexts and specific cellular roles of LRRK2 that are disrupted in PD.

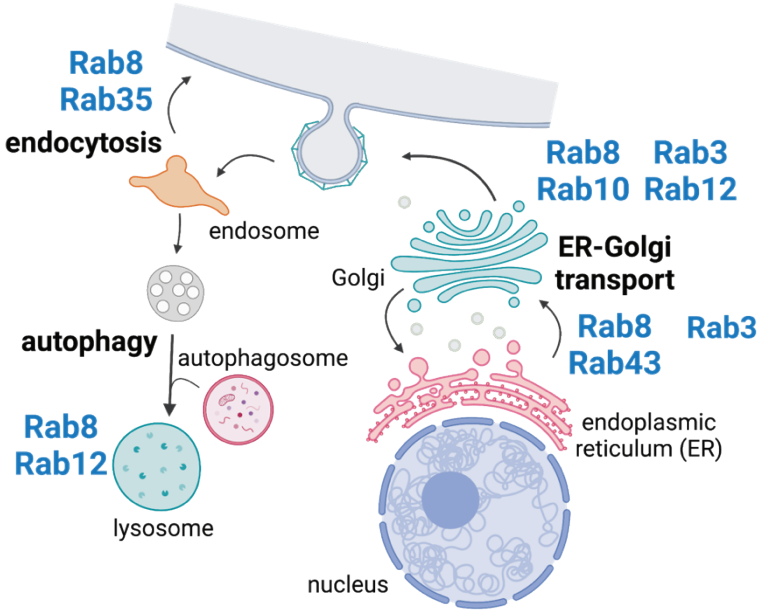

Figure 1.2: LRRK2 phosphorylates a subset of Rab GTPases with functions across the endo-lysosomal system. Simplified diagram of several endo-lysosomal trafficking pathways, including endocytosis, autophagy, and ER-Golgi transport (black, bolded). Rab GTPases endogenously phosphorylated by LRRK2 are overlaid on pathways in which they have reported functions (blue, bolded).[25,27,36] Several LRRK2 substrates function within multiple endo-lysosomal pathways. Individual isoforms of Rab3 (Rab3A/B/C/D) and Rab8 (Rab8A/B) each have evidence of endogenous phosphorylation by LRRK2 but are not depicted here for simplicity. Figure created with BioRender.com.

Despite uncertainty around the precise cellular role of LRRK2, all pathogenic LRRK2 mutations clearly lead to increased substrate phosphorylation in cells. Thus, inhibiting LRRK2 kinase activity is a compelling potential therapeutic strategy for PD. Furthermore, LRRK2 kinase inhibition has the potential to benefit even patients without a LRRK2 mutation given its clinical similarity to idiopathic PD and the intriguing observation of increased LRRK2 activity in idiopathic PD patients.[5,10] Indeed, suppressing LRRK2 activity is currently being pursued in clinical trials by multiple companies, albeit via distinct strategies. First, Ionis Pharmaceuticals, in partnership with Biogen, is running a Phase 1 clinical trial to assess the safety of a LRRK2-targeting antisense oligonucleotide (ASO), with results expected by the end of 2023.[2] ASOs work by binding to a specific mRNA sequence and suppressing translation of the target protein, thereby reducing its expression. Second, Denali Therapeutics, also in partnership with Biogen, is conducting a Phase 2b clinical trial (LUMA) for the small molecule LRRK2 kinase inhibitor BIIB122.[38] Although initial safety concerns surfaced regarding effects of small molecule LRRK2 kinase inhibition on lung histopathology, it is now thought that these are benign and reversible effects seen only at high treatment doses.[38] Results from the BIIB122 LUMA trial are expected to read out in 2025.

Finally, several additional proteins that are genetically associated with PD (including Rab29 and VPS35) are in common pathways with LRRK2, providing additional support for the critical role of LRRK2 activity in PD. First, the *RAB29* gene is located within the PARK16 locus, which is associated with increased risk of developing PD.[39] Rab29 has been shown to physically bind to LRRK2, phosphorylate LRRK2, and recruit LRRK2 to the Golgi complex, primarily utilizing assays in which Rab29, LRRK2, or both proteins are overexpressed.[14] The physiological relevance of this interaction when the proteins are expressed at endogenous levels has been questioned. Recent studies have demonstrated that knockout of endogenous Rab29 does not affect LRRK2 pathway activity in mice, and that endogenous Rab29 is not

required for localization or activation of LRRK2 on intracellular membranes.[40,41] Nevertheless, it remains possible that Rab29 and LRRK2 interact physiologically in specific cell types or conditions. Second, one mutation in the VPS35 protein (D620N) is rare, yet causal for PD.[42] VPS35 is a component of the cellular retromer complex, which functions at endosomal membranes to facilitate cargo sorting and trafficking to the Golgi or plasma membrane.[42] Recent work has demonstrated that the pathogenic D620N mutation in VPS35 enhances LRRK2 kinase activity in mouse and human cells, evidenced by an increase in Rab phosphorylation.[43] The mechanism by which this increase in LRRK2 activity occurs is unknown but could involve either direct interaction of VPS35 with LRRK2 or indirect interaction through an unknown intermediate regulator.[43] Additional proteins mutated in PD (including GBA, a lysosomal hydrolase, and α-synuclein, a presynaptic protein and the major component of Lewy bodies in PD) reportedly interact with LRRK2 as well, though likely via indirect mechanisms.[44,45] Overall, these findings show that several proteins genetically associated with PD operate within common LRRK2 signaling pathways, often within the context of intracellular trafficking and lysosomal function.

1.3 Summary

Despite the progress made in untangling the complex biology surrounding LRRK2 function since its discovery over 20 years ago, there are many questions still to be addressed. In particular, the wide range of potential roles suggested for LRRK2 have made it challenging to narrow in on those most relevant for PD pathogenesis. For example, which of the numerous cellular pathways in which LRRK2 is reported to function are at the root of neurodegeneration in PD? Furthermore, in which cell types are these dysfunctional pathways most important in the disease? It is possible that LRRK2 controls multiple, separate signaling pathways that each function only within specific cell types or cellular conditions. Alternatively, LRRK2 could be a central component of a conserved cellular pathway that has multiple possible inputs and outputs depending on the cellular context.[37] Finally, the majority of LRRK2 studies have focused on the

protein's kinase activity. How do changes to the GTPase activity of LRRK2 affect the protein's cellular function? It is plausible that LRRK2 GTPase domain mutations act via a mechanism distinct from that of kinase domain mutations, especially given the differences in cellular Rab phosphorylation levels and disease penetrance described between pathogenic mutations in each of the two domains.[20,38] In the next chapter, I attempt to address this last question by investigating how distinct LRRK2 mutations affect the protein's cellular localization and observed kinase activity.

1.4 References

1. Teymourian, H., Tehrani, F., Longardner, K., Mahato, K., Podhajny, T., Moon, J.-M., Kotagiri, Y.G., Sempionatto, J.R., Litvan, I., and Wang, J. (2022). Closing the loop for patients with Parkinson disease: where are we? Nat. Rev. Neurol. *18*, 497–507. https://doi.org/10.1038/s41582-022-00674-1.

2. Azeggagh, S., and Berwick, D.C. (2022). The development of inhibitors of leucine-rich repeat kinase 2 (LRRK2) as a therapeutic strategy for Parkinson's disease: the current state of play. Brit J Pharmacol *179*, 1478–1495. https://doi.org/10.1111/bph.15575.

3. Verstraeten, A., Theuns, J., and Broeckhoven, C.V. (2015). Progress in unraveling the genetic etiology of Parkinson disease in a genomic era. Trends Genet. *31*, 140–149. https://doi.org/10.1016/j.tig.2015.01.004.

4. Funayama, M., Nishioka, K., Li, Y., and Hattori, N. (2023). Molecular genetics of Parkinson's disease: Contributions and global trends. J. Hum. Genet. *68*, 125–130. https://doi.org/10.1038/s10038-022-01058-5.

5. Maio, R.D., Hoffman, E.K., Rocha, E.M., Keeney, M.T., Sanders, L.H., Miranda, B.R.D., Zharikov, A., Laar, A.V., Stepan, A.F., Lanz, T.A., et al. (2018). LRRK2 activation in idiopathic Parkinson's disease. Sci Transl Med *10*, eaar5429. https://doi.org/10.1126/scitranslmed.aar5429.

6. Armstrong, M.J., and Okun, M.S. (2020). Diagnosis and Treatment of Parkinson Disease. JAMA *323*, 548–560. https://doi.org/10.1001/jama.2019.22360.

7. Shahmoradian, S.H., Lewis, A.J., Genoud, C., Hench, J., Moors, T.E., Navarro, P.P., Castaño-Díez, D., Schweighauser, G., Graff-Meyer, A., Goldie, K.N., et al. (2019). Lewy

pathology in Parkinson's disease consists of crowded organelles and lipid membranes. Nat Neurosci *22*, 1099–1109. https://doi.org/10.1038/s41593-019-0423-2.

8. Tolosa, E., Vila, M., Klein, C., and Rascol, O. (2020). LRRK2 in Parkinson disease: challenges of clinical trials. Nat Rev Neurol, 1–11. https://doi.org/10.1038/s41582-019-0301-2.

9. Taylor, M., and Alessi, D.R. (2020). Advances in elucidating the function of leucine-rich repeat protein kinase-2 in normal cells and Parkinson's disease. Curr Opin Cell Biol *63*, 102–113. https://doi.org/10.1016/j.ceb.2020.01.001.

10. Rocha, E.M., Keeney, M.T., Maio, R.D., Miranda, B.R.D., and Greenamyre, J.T. (2022). LRRK2 and idiopathic Parkinson's disease. Trends Neurosci. https://doi.org/10.1016/j.tins.2021.12.002.

11. Paisán-Ruíz, C., Jain, S., Evans, E.W., Gilks, W.P., Simón, J., Brug, M. van der, Munain, A.L. de, Aparicio, S., Gil, A.M., Khan, N., et al. (2004). Cloning of the Gene Containing Mutations that Cause PARK8-Linked Parkinson's Disease. Neuron *44*, 595–600. https://doi.org/10.1016/j.neuron.2004.10.023.

12. Zimprich, A., Biskup, S., Leitner, P., Lichtner, P., Farrer, M., Lincoln, S., Kachergus, J., Hulihan, M., Uitti, R.J., Calne, D.B., et al. (2004). Mutations in LRRK2 Cause Autosomal-Dominant Parkinsonism with Pleomorphic Pathology. Neuron *44*, 601–607. https://doi.org/10.1016/j.neuron.2004.11.005.

13. Funayama, M., Hasegawa, K., Kowa, H., Saito, M., Tsuji, S., and Obata, F. (2002). A new locus for Parkinson's disease (PARK8) maps to chromosome 12p11.2–q13.1. Ann. Neurol. *51*, 296–301. https://doi.org/10.1002/ana.10113.

14. Berwick, D.C., Heaton, G.R., Azeggagh, S., and Harvey, K. (2019). LRRK2 Biology from structure to dysfunction: research progresses, but the themes remain the same. Mol Neurodegener *14*, 49. https://doi.org/10.1186/s13024-019-0344-2.

15. Berger, Z., Smith, K.A., and LaVoie, M.J. (2010). Membrane Localization of LRRK2 Is Associated with Increased Formation of the Highly Active LRRK2 Dimer and Changes in Its Phosphorylation. Biochemistry-us *49*, 5511–5523. https://doi.org/10.1021/bi100157u.

16. Zhu, H., Tonelli, F., Alessi, D.R., and Sun, J. (2022). Structural basis of human LRRK2 membrane recruitment and activation. Biorxiv, 2022.04.26.489605. https://doi.org/10.1101/2022.04.26.489605.

17. Rideout, H.J., Chartier-Harlin, M.-C., Fell, M.J., Hirst, W.D., Huntwork-Rodriguez, S., Leyns, C.E.G., Mabrouk, O.S., and Taymans, J.-M. (2020). The Current State-of-the Art of LRRK2-Based Biomarker Assay Development in Parkinson's Disease. Front. Neurosci. *14*, 865. https://doi.org/10.3389/fnins.2020.00865.

18. Miklossy, J., Arai, T., Guo, J.-P., Klegeris, A., Yu, S., McGeer, E.G., and McGeer, P.L. (2006). LRRK2 Expression in Normal and Pathologic Human Brain and in Human Cell Lines. J. Neuropathol. Exp. Neurol. *65*, 953–963. https://doi.org/10.1097/01.jnen.0000235121.98052.54.

19. Kalogeropulou, A.F., Purlyte, E., Tonelli, F., Lange, S.M., Wightman, M., Prescott, A.R., Padmanabhan, S., Sammler, E., and Alessi, D.R. (2022). Impact of 100 LRRK2 variants linked to Parkinson's disease on kinase activity and microtubule binding. Biochem J *479*, 1759–1783. https://doi.org/10.1042/bcj20220161.

20. Iannotta, L., Biosa, A., Kluss, J.H., Tombesi, G., Kaganovich, A., Cogo, S., Plotegher, N., Civiero, L., Lobbestael, E., Baekelandt, V., et al. (2020). Divergent Effects of G2019S and R1441C LRRK2 Mutations on LRRK2 and Rab10 Phosphorylations in Mouse Tissues. Cells *9*, 2344. https://doi.org/10.3390/cells9112344.

21. Haugarvoll, K., Rademakers, R., Kachergus, J.M., Nuytemans, K., Ross, O.A., Gibson, J.M., Tan, E.-K., Gaig, C., Tolosa, E., Goldwurm, S., et al. (2008). Lrrk2 R1441C parkinsonism is clinically similar to sporadic Parkinson disease. Neurology *70*, 1456–1460. https://doi.org/10.1212/01.wnl.0000304044.22253.03.

22. Lee, A.J., Wang, Y., Alcalay, R.N., Mejia-Santana, H., Saunders-Pullman, R., Bressman, S., Corvol, J., Brice, A., Lesage, S., Mangone, G., et al. (2017). Penetrance estimate of LRRK2 p.G2019S mutation in individuals of non-Ashkenazi Jewish ancestry: LRRK2 Mutation in Non-Ashkenazi Jewish Ancestry. Movement Disord *32*, 1432–1438. https://doi.org/10.1002/mds.27059.

23. Ruiz-Martínez, J., Gorostidi, A., Ibañez, B., Alzualde, A., Otaegui, D., Moreno, F., Munain, A.L. de, Bergareche, A., Gómez-Esteban, J.C., and Massó, J.F.M. (2010). Penetrance in Parkinson's disease related to the LRRK2 R1441G mutation in the Basque country (Spain). Movement Disord *25*, 2340–2345. https://doi.org/10.1002/mds.23278.

24. Steger, M., Tonelli, F., Ito, G., Davies, P., Trost, M., Vetter, M., Wachter, S., Lorentzen, E., Duddy, G., Wilson, S., et al. (2016). Phosphoproteomics reveals that Parkinson's disease kinase LRRK2 regulates a subset of Rab GTPases. Elife *5*, e12813. https://doi.org/10.7554/elife.12813.

25. Steger, M., Diez, F., Dhekne, H.S., Lis, P., Nirujogi, R.S., Karayel, O., Tonelli, F., Martinez, T.N., Lorentzen, E., Pfeffer, S.R., et al. (2017). Systematic proteomic analysis of LRRK2-mediated Rab GTPase phosphorylation establishes a connection to ciliogenesis. Elife *6*, e31012. https://doi.org/10.7554/elife.31012.

26. Pfeffer, S.R. (2018). LRRK2 and Rab GTPases. Biochem Soc T *46*, 1707–1712. https://doi.org/10.1042/bst20180470.

27. Kiral, F.R., Kohrs, F.E., Jin, E.J., and Hiesinger, P.R. (2018). Rab GTPases and Membrane Trafficking in Neurodegeneration. Curr Biol *28*, R471–R486. https://doi.org/10.1016/j.cub.2018.02.010.

28. Bonet-Ponce, L., and Cookson, M.R. (2021). LRRK2 recruitment, activity, and function in organelles. Febs J. https://doi.org/10.1111/febs.16099.

29. Eguchi, T., Kuwahara, T., Sakurai, M., Komori, T., Fujimoto, T., Ito, G., Yoshimura, S., Harada, A., Fukuda, M., Koike, M., et al. (2018). LRRK2 and its substrate Rab GTPases are sequentially targeted onto stressed lysosomes and maintain their homeostasis. Proc National Acad Sci *115*, 201812196. https://doi.org/10.1073/pnas.1812196115.

30. Liu, Z., Xu, E., Zhao, H.T., Cole, T., and West, A.B. (2020). LRRK2 and Rab10 coordinate macropinocytosis to mediate immunological responses in phagocytes. Embo J *39*, e104862. https://doi.org/10.15252/embj.2020104862.

31. Bonet-Ponce, L., Beilina, A., Williamson, C.D., Lindberg, E., Kluss, J.H., Saez-Atienzar, S., Landeck, N., Kumaran, R., Mamais, A., Bleck, C.K.E., et al. (2020). LRRK2 mediates tubulation and vesicle sorting from lysosomes. Sci Adv *6*, eabb2454. https://doi.org/10.1126/sciadv.abb2454.

32. Liu, Z., Bryant, N., Kumaran, R., Beilina, A., Abeliovich, A., Cookson, M.R., and West, A.B. (2017). LRRK2 phosphorylates membrane-bound Rabs and is activated by GTP-bound Rab7L1 to promote recruitment to the trans-Golgi network. Hum Mol Genet *27*, 385–395. https://doi.org/10.1093/hmg/ddx410.

33. Kluss, J.H., Beilina, A., Williamson, C.D., Lewis, P.A., Cookson, M.R., and Bonet-Ponce, L. (2022). Lysosomal positioning regulates Rab10 phosphorylation at LRRK2+ lysosomes. P Natl Acad Sci Usa *119*, e2205492119. https://doi.org/10.1073/pnas.2205492119.

34. Gomez, R.C., Wawro, P., Lis, P., Alessi, D.R., and Pfeffer, S.R. (2019). Membrane association but not identity is required for LRRK2 activation and phosphorylation of Rab GTPases. J Cell Biology *218*, 4157–4170. https://doi.org/10.1083/jcb.201902184.

35. Purlyte, E., Dhekne, H.S., Sarhan, A.R., Gomez, R., Lis, P., Wightman, M., Martinez, T.N., Tonelli, F., Pfeffer, S.R., and Alessi, D.R. (2018). Rab29 activation of the Parkinson's disease-associated LRRK2 kinase. Embo J *37*, 1–18. https://doi.org/10.15252/embj.201798099.

36. Hur, E.-M., Jang, E.-H., Jeong, G.R., and Lee, B.D. (2019). LRRK2 and membrane trafficking: nexus of Parkinson's disease. Bmb Rep *52*, 533–539. https://doi.org/10.5483/bmbrep.2019.52.9.186.

37. Lewis, P.A., and Manzoni, C. (2012). LRRK2 and human disease: a complicated question or a question of complexes? Sci Signal *5*, pe2. https://doi.org/10.1126/scisignal.2002680.

38. West, A. B., and Schwarzschild, M.A. (2023). LRRK2-Targeting Therapies March Through the Valley of Death. Movement Disorders, *38*, 361-365. https://doi.org/10.1002/mds.29343.

39. Satake, W., Nakabayashi, Y., Mizuta, I., Hirota, Y., Ito, C., Kubo, M., Kawaguchi, T., Tsunoda, T., Watanabe, M., Takeda, A., et al. (2009). Genome-wide association study identifies common variants at four loci as genetic risk factors for Parkinson's disease. Nat. Genet. *41*, 1303–1307. https://doi.org/10.1038/ng.485.

40. Kalogeropulou, A.F., Freemantle, J.B., Lis, P., Vides, E.G., Polinski, N.K., and Alessi, D.R. (2020). Endogenous Rab29 does not impact basal or stimulated LRRK2 pathway activity. Biochem. J. *477*, 4397–4423. https://doi.org/10.1042/bcj20200458.

41. Kluss, J.H., Bonet-Ponce, L., Lewis, P.A., and Cookson, M.R. (2022). Directing LRRK2 to membranes of the endolysosomal pathway triggers RAB phosphorylation and JIP4 recruitment. Neurobiol. Dis. *170*, 105769. https://doi.org/10.1016/j.nbd.2022.105769.

42. Williams, E.T., Chen, X., Otero, P.A., and Moore, D.J. (2022). Understanding the contributions of VPS35 and the retromer in neurodegenerative disease. Neurobiol. Dis. *170*, 105768. https://doi.org/10.1016/j.nbd.2022.105768.

43. Mir, R., Tonelli, F., Lis, P., Macartney, T., Polinski, N.K., Martinez, T.N., Chou, M.-Y., Howden, A.J.M., König, T., Hotzy, C., et al. (2018). The Parkinson's disease VPS35[D620N] mutation enhances LRRK2-mediated Rab protein phosphorylation in mouse and human. Biochem J *475*, 1861–1883. https://doi.org/10.1042/bcj20180248.

44. Cresto, N., Gardier, C., Gubinelli, F., Gaillard, M., Liot, G., West, A.B., and Brouillet, E. (2019). The unlikely partnership between LRRK2 and α-synuclein in Parkinson's disease. Eur J Neurosci *49*, 339–363. https://doi.org/10.1111/ejn.14182.

45. Ysselstein, D., Nguyen, M., Young, T.J., Severino, A., Schwake, M., Merchant, K., and Krainc, D. (2019). LRRK2 kinase activity regulates lysosomal glucocerebrosidase in neurons derived from Parkinson's disease patients. Nat. Commun. *10*, 5570. https://doi.org/10.1038/s41467-019-13413-w.

Chapter 2:

Dissecting the effects of GTPase and kinase domain mutations on LRRK2 endosomal localization and activity

2.1 Abstract

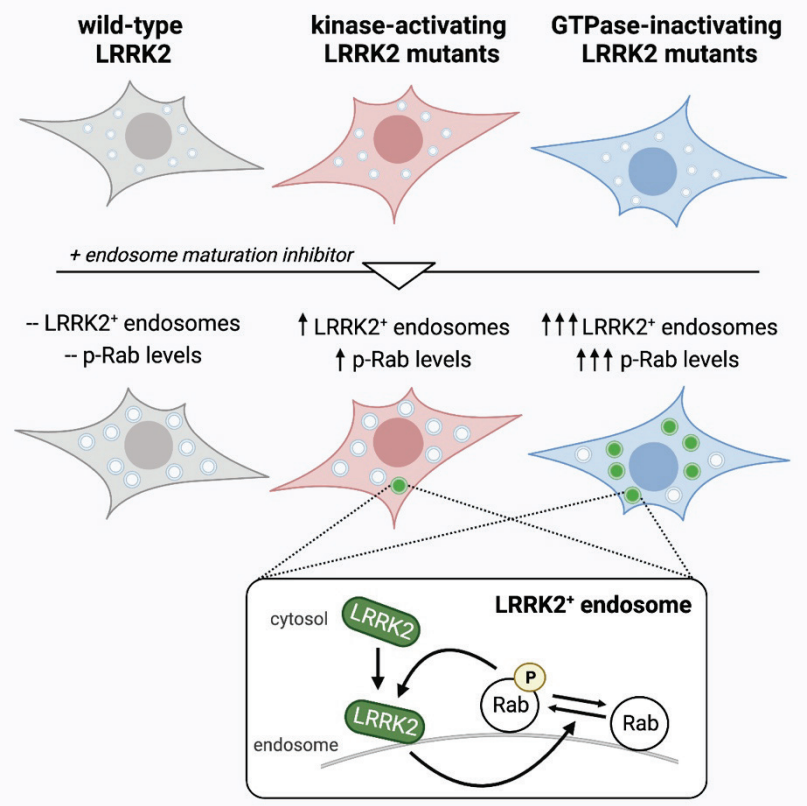

Figure 2.1: Graphical abstract for Chapter 2.

Parkinson's disease-causing leucine-rich repeat kinase 2 (LRRK2) mutations lead to varying degrees of Rab GTPase hyperphosphorylation. Puzzlingly, LRRK2 GTPase-inactivating mutations—which do not affect intrinsic kinase activity—lead to higher levels of cellular Rab phosphorylation than kinase-activating mutations. Here, we investigate whether mutation-dependent differences in LRRK2 cellular localization could explain this discrepancy. We discover that blocking endosomal maturation leads to the rapid formation of mutant LRRK2^{+} endosomes on which LRRK2 phosphorylates substrate Rabs. LRRK2^{+} endosomes are maintained through positive feedback, which mutually reinforces membrane localization of LRRK2 and phosphorylated Rab substrates. Furthermore, across a panel of mutants, cells

expressing GTPase-inactivating mutants form strikingly more LRRK2^{+} endosomes than cells expressing kinase-activating mutants, resulting in higher total cellular levels of phosphorylated Rabs. Our study suggests that the increased probability that LRRK2 GTPase-inactivating mutants are retained on intracellular membranes compared to kinase-activating mutants leads to higher substrate phosphorylation.

2.2 Introduction

Mutations in leucine-rich repeat kinase 2 (LRRK2) are the most prevalent known cause of Parkinson's disease (PD).[1–3] LRRK2 comprises several protein domains, including catalytic GTPase and kinase domains, as well as non-catalytic domains believed to mediate protein-protein interactions (**Figure 2.2A**). Disease-causing mutations in the kinase domain, including the most common disease-causing LRRK2 mutation G2019S, can increase the intrinsic (*in vitro*) kinase activity of LRRK2.[4–8] Disease-causing mutations in the GTPase domain, including the highly penetrant LRRK2 mutation R1441G, can decrease the GTPase activity of LRRK2 without altering *in vitro* kinase activity.[7–10] Surprisingly, in cells, these LRRK2 GTPase-inactivating mutations lead to higher phosphorylation levels of its Rab GTPase substrates than the kinase-activating mutations.[8,11]

In fact, all disease-causing LRRK2 mutations lead to increased phosphorylation of its Rab GTPase substrates in cells.[11,12] Both LRRK2 and Rab GTPases function on vesicles within the endo-lysosomal system and cycle between cytoplasmic and membrane-bound states.[13] Though largely cytoplasmic, LRRK2 can associate with vesicular membranes to phosphorylate membrane-bound Rabs.[14–17] In some conditions, such as prolonged lysosomal damage, LRRK2 has been shown to be retained on intracellular membranes to a level that can be readily observed by microscopy.[16,18–21] How different LRRK2 mutants affect its membrane association and Rab phosphorylation remains poorly characterized.

Here, we developed a cellular system to dissect the impact of LRRK2 mutations on LRRK2 cellular localization and substrate phosphorylation. We found that acutely blocking endosomal maturation led to the formation of LRRK2-positive endosomes (LRRK2$^+$ endosomes) in cells expressing mutant forms of LRRK2. We demonstrated that positive feedback is operating on the LRRK2$^+$ endosomes to mutually reinforce the membrane localization of LRRK2 and phosphorylated Rab substrates. Interestingly, across a panel of disease-associated LRRK2 mutants, cell populations expressing GTPase-inactivating mutants formed more LRRK2$^+$ endosomes in a dramatically larger fraction of cells than cell populations expressing kinase-activating mutants. Furthermore, the amount of LRRK2$^+$ endosomes observed was highly correlated with cellular Rab phosphorylation levels across the panel of mutants. Together, we propose a model wherein LRRK2 GTPase-inactivating mutants have a higher propensity than kinase-activating mutants to form LRRK2$^+$ endosomes, thereby providing an explanation for stronger increases in overall cellular Rab phosphorylation.

2.3 Results

2.3.1 Establishment of a cellular system to monitor, quantify, and compare LRRK2 localization across mutants

To monitor cellular LRRK2 localization, we used a doxycycline-inducible system allowing GFP-tagged LRRK2 plasmids to be stably expressed at relatively low, consistent levels.[7,22–24] We started with three cell lines, expressing wild-type (WT), G2019S, or R1441G LRRK2 (**Figure 2.2A**). As previously reported, in control conditions, LRRK2 expression was largely diffuse and similar between WT and mutant cell lines, though a fraction of R1441G LRRK2 cells contained small cytoplasmic LRRK2 puncta (**Figure 2.2B**).[7,25]

We searched for a chemical perturbation that would amplify differences in LRRK2 localization across mutants and WT. We reasoned that blocking vesicle trafficking could enrich

for a pool of vesicles on which LRRK2 normally signals, thereby amplifying LRRK2 vesicle association events. To test this hypothesis, we evaluated six compounds inhibiting several

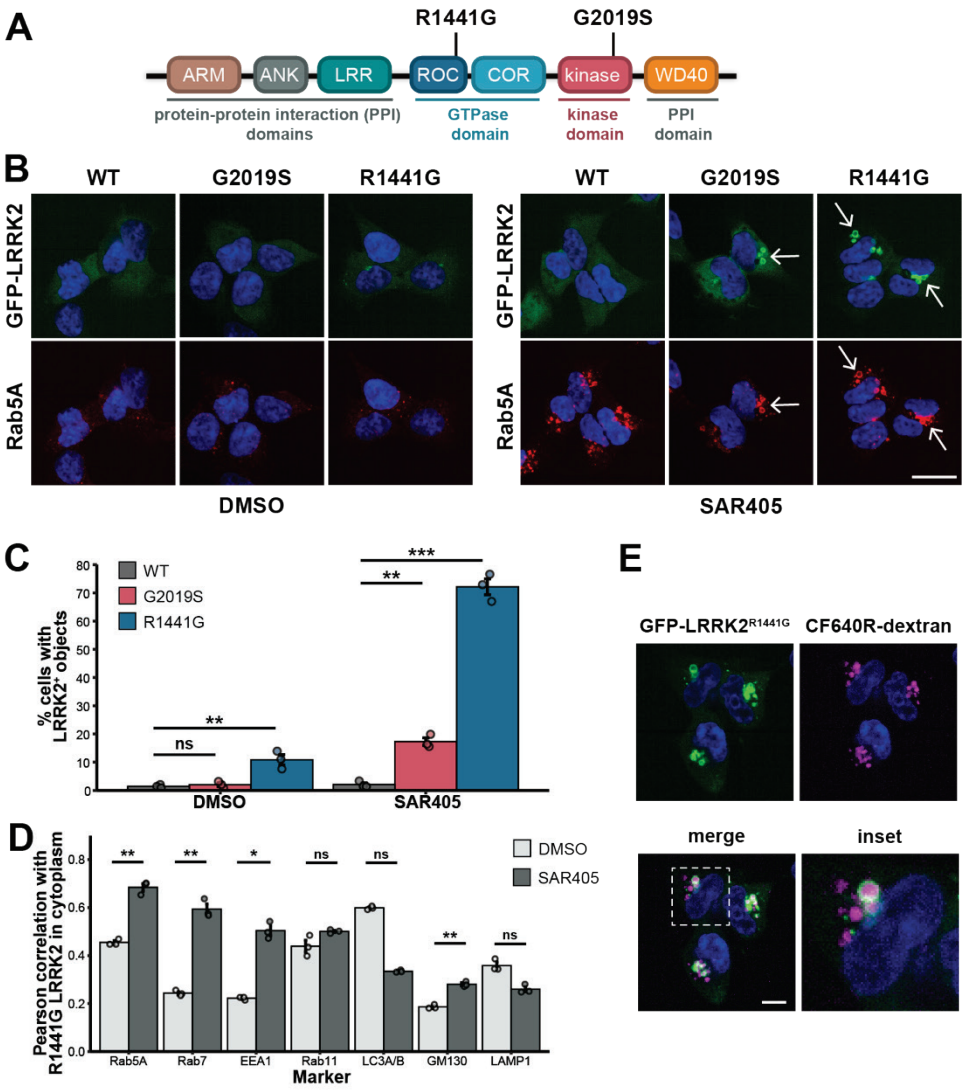

Figure 2.2: VPS34 inhibition reveals mutant-dependent LRRK2 localization on enlarged endosomes. (A) LRRK2 domain structure highlighting two Parkinson's disease-causing mutations in the Roc-COR GTPase domain (R1441G) and the kinase domain (G2019S). **(B)** Representative images of GFP-LRRK2 variants expressed in stably transfected T-REx HEK293 cells. Cells were treated for 30 min with DMSO or SAR405 (3 μM) before immunostaining for Rab5A. Arrows indicate localization of LRRK2 mutants on vesicular structures in SAR405. Scale bar, 25 μm. **(C)** Quantification of the percent of cells with LRRK2 localized on vesicular structures after 30 min treatment with DMSO or SAR405 (3 μM). Statistical significance was calculated via one-way ANOVA followed by Dunnett's post hoc test (n = 3 wells, >90 cells per well). **(D)** Co-localization analysis of GFP-tagged R1441G LRRK2 with early endosome (Rab5A, EEA1), late endosome (Rab7), recycling endosome (Rab11), autophagosome (LC3A/B), Golgi complex (GM130), or lysosome (LAMP1) markers after 30 min treatment with DMSO or

(caption continued from previous page) SAR405 (3 μM). Each point represents the mean of single-cell measurements for all imaged cells within a well. Statistical significance of increased correlation was calculated via unpaired, one-tailed t test with Bonferroni correction (n = 3 wells, >90 cells per well). **(E)** Representative images of stable T-REx HEK293 cells expressing GFP-tagged R1441G LRRK2 labeled with 10 kDa CF640R-dextran in the presence of SAR405 (3 μM). Live cell images shown are from 30 min after washout of excess dextran to assess localization. Scale bar, 10 μm. Error bars: mean ± SEM. *p < 0.05; **p < 0.01; ***p < 0.001.

endo-lysosomal pathways as LRRK2 has functions at multiple stages of vesicle trafficking (**Figure A.1A**).[26,27]

Quantification of single-cell phenotypes showed that both chloroquine and SAR405 significantly altered LRRK2 localization for both mutants (**Figure A.1A**). We chose to further investigate the VPS34 inhibitor SAR405, as this perturbation significantly altered only mutant but not WT LRRK2 localization (**Figure A.1A**). Upon VPS34 inhibition, the LRRK2 mutant cells had enlarged, LRRK2$^+$ vesicular structures (**Figure 2.2B**). Strikingly, R1441G, compared with G2019S, LRRK2-expressing cell populations had a higher proportion of cells containing LRRK2$^+$ vesicles (72% vs. 17%) (**Figure 2.2C**). Overall, VPS34 inhibition revealed strong differences in enrichment on vesicles between WT and mutant LRRK2, as well as between LRRK2 mutants.

How does VPS34 inhibition affect vesicle trafficking? VPS34 is a phosphoinositide 3-kinase (PI3K) that generates PI(3)P, which promotes maturation of early endosomes.[28] We verified in our system that VPS34 inhibition reduced PI(3)P fluorescence on endosomes (**Figures A.1B-C**).[29,30] Furthermore, across WT and mutant LRRK2 cells, VPS34 inhibition increased the total area of objects positive for early endosomal protein Rab5A (**Figures 2.2B and A.1D**).[28,31] Thus, VPS34 inhibition increases the cellular pool of maturing, Rab5$^+$ endosomal membranes.

To characterize the LRRK2$^+$ vesicles induced by VPS34 inhibition, we focused on the strong R1441G phenotype (conclusions are similar for G2019S; data not shown). We found strong colocalization of R1441G LRRK2 with early to late endosome markers (EEA1, Rab5A,

Rab7). These strongly co-localized markers had both a high Pearson correlation in VPS34 inhibition conditions and a significant increase in Pearson correlation from DMSO upon VPS34 inhibition (**Figures 2.2D, A.2A-B**). Further, labeled dextran added to the extracellular medium of SAR405-treated cells was present within LRRK2$^+$ vesicles (**Figure 2.2E**). Overall, we reasoned that the LRRK2$^+$ vesicles revealed by SAR405 treatment are a subset of enlarged, intermediate vesicles maturing from early (EEA1, Rab5) to late (Rab7) endosomal identity that are capable of transporting endocytic cargo.

Taken together, blocking endosomal maturation via VPS34 inhibition increased the pool of enlarged, maturing endosomes, which revealed differentially amplified LRRK2 endosomal localization across mutants. This provided a setting in which to compare the formation of LRRK2$^+$ endosomes and downstream consequences across mutants.

2.3.2 Cells expressing R1441G LRRK2 form more LRRK2$^+$ endosomes than cells expressing G2019S LRRK2

We next investigated mutant specific LRRK2$^+$ endosome formation in response to acute VPS34 inhibition using video microscopy. For R1441G LRRK2, most cells developed LRRK2$^+$ endosomes within 10 min. In contrast, for G2019S LRRK2, only a modest proportion of cells with LRRK2$^+$ endosomes were observed. WT LRRK2$^+$ endosomes were only observed in a very small proportion (1%–3%) of cells (**Figures 2.3A-B**). The fraction of cells with LRRK2$^+$ endosomes was stable over the remainder of the one-hour observation period. Overall, acute VPS34 inhibition induced more rapid LRRK2$^+$ endosome formation in a larger proportion of cells expressing R1441G LRRK2 compared with G2019S LRRK2.

We further examined the subpopulation of cells containing mutant LRRK2$^+$ endosomes. After acute VPS34 inhibition, LRRK2$^+$ endosomes are first visible as small, punctate structures

that become enlarged over time, often resulting from apparent fusion of multiple endosomes.

The average LRRK2 intensity on endosomes for R1441G LRRK2 was slightly increased

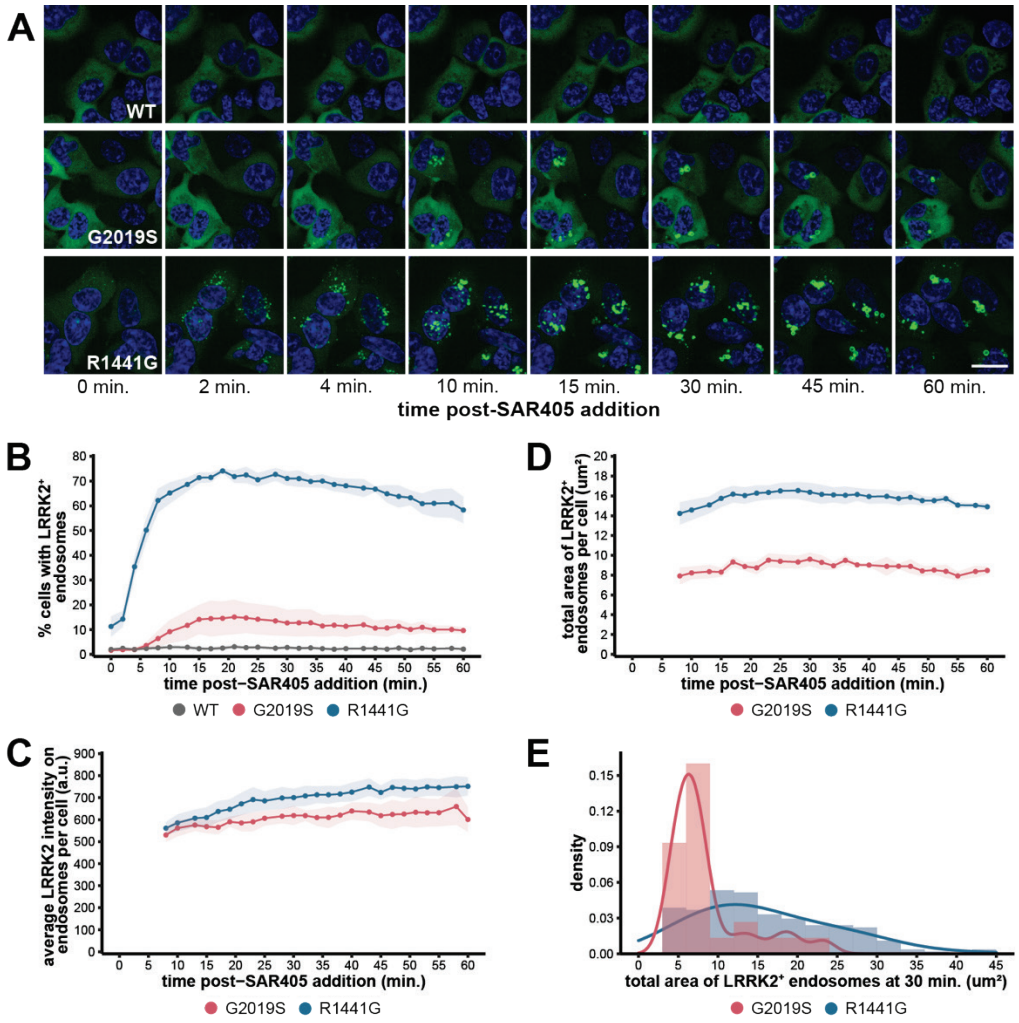

Figure 2.3: Distinct LRRK2 mutations lead to differential levels of LRRK2⁺ endosome formation. **(A)** Representative sequential images of live stable T-REx HEK293 cells expressing the indicated GFP-LRRK2 variants treated with SAR405 (3 μM). Cells were imaged approximately every 2 min. Scale bar, 25 μm. **(B)** Quantification of percent of cells with LRRK2⁺ endosomes. **(C and D)** Quantification of the average GFP-LRRK2 intensity on endosomes (C) or the total area of LRRK2⁺ endosomes (D) per cell for cells in (B) containing LRRK2⁺ endosomes. Time points in which G2019S LRRK2 was not yet localized to endosomes were omitted. (B–D) Shaded areas: mean ± SEM, n = 4 independent experiments, >200 cells per LRRK2 genotype in each experiment). **(E)** Single-cell distributions of the total area of LRRK2⁺ endosomes per cell after 30 min of SAR405 treatment (3 μM) (n = 25 cells G2019S, 181 cells R1441G). (C–E) The number of cells with WT LRRK2 endosome localization was too few for quantification.

compared with G2019S LRRK2 (**Figure 2.3C**) (though quantification at later time points may have been biased due to increased R1441G LRRK2$^+$ endosome clustering; **Figure 2.3A**). By quantifying the total area of LRRK2$^+$ endosomes per cell, we found that R1441G LRRK2 associated with a larger endosomal mass than G2019S LRRK2 (**Figures 2.3A, 2.3D-E**).

As controls, we tested that DMSO treatment did not alter LRRK2 localization (**Figure A.1E**); SAR405 treatment did not induce significant changes in localization of GFP in cells expressing an empty vector control; and a structurally distinct VPS34 inhibitor, VPS34-IN1, induced similar phenotypes across LRRK2 mutant cell lines (**Figure A.1F**). In summary, upon acute VPS34 inhibition, the GTPase-inactivating mutant R1441G has a larger area of LRRK2$^+$ endosomes in a larger proportion of cells than the kinase-activating mutant G2019S.

2.3.3 LRRK2$^+$ endosome formation leads to amplified cellular Rab phosphorylation levels

We next investigated the localization and phosphorylation of known LRRK2 Rab GTPase substrates[12,14,15] upon VPS34 inhibition. We focused on Rab10, Rab8A, and Rab35.

Consistent with previous reports, under control conditions, the p-Rab10 signal was greater for cells expressing R1441G LRRK2 and to a lesser extent G2019S LRRK2 than for WT LRRK2, and these signals were abolished after treatment with the LRRK2 kinase inhibitor MLi-2[11] (**Figures 2.4A-B**). After acute VPS34 inhibition, p-Rab10 levels were consistently amplified across the mutant cell populations by 3-fold, while total Rab10 signal remained largely unchanged (**Figures 2.4A-B, A.3A-B**). Importantly, the levels of p-Rab10 decreased to baseline after treatment with MLi-2, confirming that the observed increases in phosphorylation were due to LRRK2 kinase activity[12] (**Figures 2.4A-B**). In fact, Rab10 and p-Rab10 strongly colocalized with R1441G (**Figures 2.4C and A.3C**) and G2019S LRRK2 (data not shown). This co-localization was apparent on LRRK2$^+$ endosomes (**Figures 2.4A and A.3C**). Within the subset

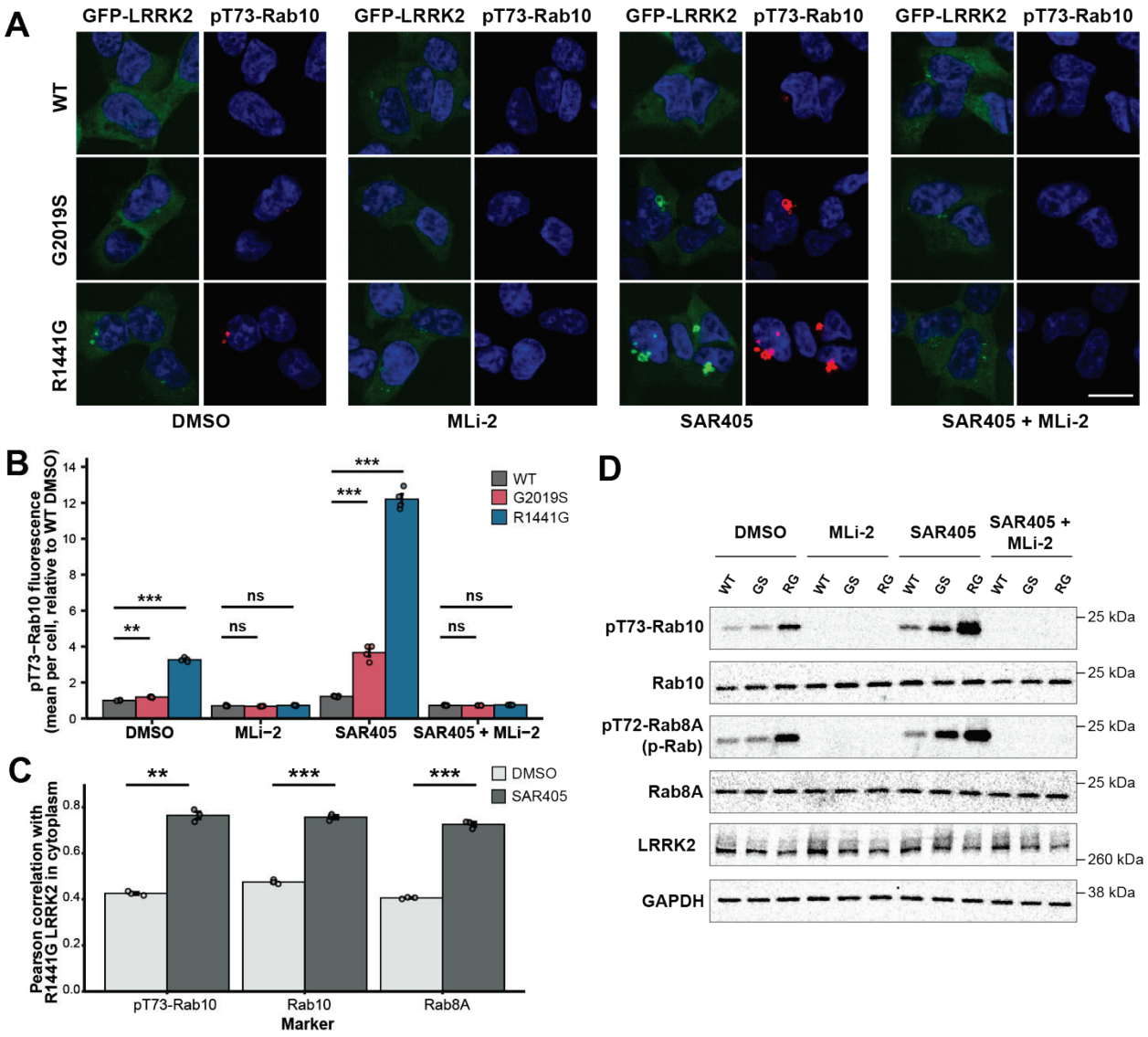

Figure 2.4: LRRK2 phosphorylates Rab10 on LRRK2⁺ endosomes. (A) Representative images of stable T-REx HEK293 cells expressing GFP-LRRK2 variants after 30 min drug treatment and immunostaining for LRRK2-specific phosphosite on Rab10 (pT73). MLi-2: 1 μM, SAR405: 3 μM. Scale bar, 20 μm. **(B)** Quantification of mean pT73-Rab10 fluorescence intensity per cell displayed as fold change relative to DMSO-treated cells expressing WT LRRK2. Each point represents the mean of single-cell measurements for all imaged cells within a well. Statistical significance was calculated via one-way ANOVA followed by Dunnett's post hoc test (n = 4 wells, >200 cells per well). **(C)** Co-localization analysis of GFP-tagged R1441G LRRK2 with pT73-Rab10, Rab10, or Rab8A after 30 min treatment with DMSO or SAR405 (3 μM). Each point represents the mean of single-cell measurements for all imaged cells within a well. Statistical significance was calculated via unpaired, one-tailed t test with Bonferroni correction (n = 3 wells, >130 cells per well). **(D)** Western blot for phosphorylated Rab10 and Rab8A after 30 min drug treatment using stable T-REx HEK293 cells expressing GFP-LRRK2 variants. We note from the manufacturer that the pT72-Rab8A antibody cross-reacts with phosphorylated Rab3A, Rab10, Rab35, and Rab43 (indicated by ''p-Rab''). MLi-2: 1 μM, SAR405: 3 μM. GS, G2019S; RG, R1441G. Error bars: mean ± SEM. **p < 0.01; ***p < 0.001..

of cells with mutant LRRK2$^+$ endosomes after VPS34 inhibition, cells with higher cellular p-Rab10 levels largely had a greater LRRK2$^+$ endosomal mass (**Figure A.3F**). The difference in pRab10 levels observed across LRRK2 mutants reflects both altered proportions of cells with LRRK2$^+$ endosomes and masses of LRRK2$^+$ endosomes within single cells. For substrates Rab8A and Rab35, we observed similar increases in phosphorylation and co-localization with LRRK2 upon VPS34 inhibition (using both western blot and phos-tag analysis to measure phosphorylation levels and IF to observe localization of total Rab8A and total Rab35; **Figures 2.4C-D, A.3C–E, and A.3G**). Overall, VPS34 inhibition revealed amplification of LRRK2 and phosphorylated substrate levels on the same LRRK2$^+$ endosomal membranes. Finally, in mouse embryonic fibroblasts (MEFs) expressing LRRK2 at endogenous levels, we similarly observed significant VPS34 inhibitor-induced increases in proportions of cells with enlarged, perinuclear vesicles positive for Rab10, p-Rab10, or Rab8A in R1441C LRRK2 knock-in MEFs and, to a lesser degree, in WT MEFs. Further, these changes in vesicle localization were sensitive to MLi-2 co-treatment (**Figures A.4A–D**).

As we observed co-localization of LRRK2 with both Rab5A and Rab7 on mutant LRRK2$^+$ endosomes (**Figures 2.2D and A.2A**), we wondered whether LRRK2 could phosphorylate these proteins in our system. Rab5A has been suggested as a potential endogenous LRRK2 substrate, and Rab7 has recently been shown to be a substrate of LRRK1.[11,12,32] However, we did not find evidence of phosphorylation of either protein by LRRK2 upon SAR405 treatment (**Figures A.3H and A.3I**), suggesting that these proteins are not endogenous LRRK2 substrates.[12]

2.3.4 LRRK2$^+$ endosomes are established and maintained through Rab phosphorylation

We next wondered whether Rab phosphorylation could play a role in maintaining LRRK2 on the membrane of LRRK2$^+$ endosomes, as binding of LRRK2 to phosphorylated Rabs was recently described *in vitro* on lipid bilayers.[33]

First, we investigated the role of Rab phosphorylation in the establishment of mutant LRRK2^{+} endosomes. Co-treatment of cells for 30 min with both the VPS34 inhibitor and the LRRK2 kinase inhibitor MLi-2 blocked the formation of LRRK2^{+} endosomes (**Figure A.5A**). To further validate this result, we overexpressed the phosphatase PPM1H, which dephosphorylates Rab proteins and counteracts LRRK2 signaling.[34] Overexpression of PPM1H dramatically decreased the proportion of cells with LRRK2^{+} endosomes formed upon VPS34 inhibition for both R1441G and G2019S LRRK2 (**Figures 2.5A-B, and A.5B**). (We confirmed that PPM1H overexpression decreased p-Rab10 levels without affecting total Rab10 levels and that overexpression of the inactive H153D PPM1H mutant had no effect on R1441G LRRK2 localization; **Figures 2.5B and A.5C**). Thus, Rab dephosphorylation inhibits the establishment of LRRK2^{+} endosomes.

Second, we investigated the role of Rab phosphorylation in the maintenance of mutant LRRK2^{+} endosomes. After 30 min of VPS34 inhibition to enrich R1441G LRRK2 on endosomes, we added DMSO or MLi-2 to the cell media and monitored LRRK2^{+} endosomes via live imaging (**Figure 2.5C**). After MLi-2 treatment, VPS34 inhibitor-induced LRRK2^{+} endosomes were rapidly lost for both R1441G and G2019S LRRK2 (**Figure 2.5C-D, and A.5D**). Thus, the ability of LRRK2 to phosphorylate Rabs is required for the maintenance of mutant LRRK2^{+} endosomes once established. Together, our results suggest that positive feedback is operating on LRRK2^{+} endosomes to maintain LRRK2 and Rab localization (**Figure 2.5E**).

We then tested whether mutating two reported Rab binding locations on R1441G LRRK2 could block mutant LRRK2^{+} endosome formation. The first site (N-terminal K17-18) binds phosphorylated Rab8 and Rab10, while the second site (K439 in the Armadillo domain) binds non-phosphorylated Rab8, Rab10, and Rab29; mutation of these sites to alanine (K17/18A) or glutamate (K439E) was reported to weaken the Rab binding affinity to LRRK2.[33] Upon VPS34

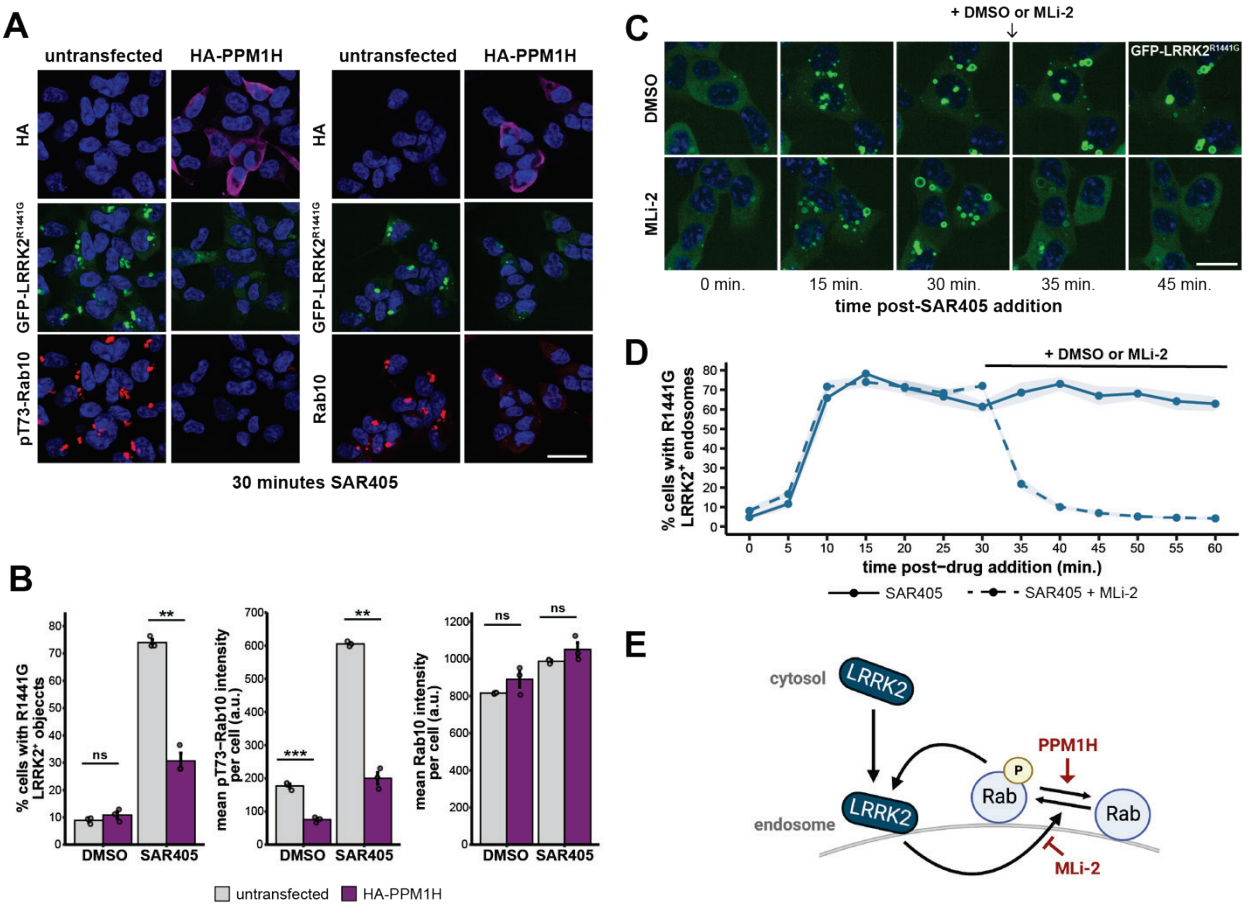

Figure 2.5: LRRK2⁺ endosomes are established and maintained through Rab phosphorylation. (A) Representative images of stable T-REx HEK293 cells expressing GFP-tagged R1441G LRRK2 and transiently transfected with a plasmid encoding HA-PPM1H. Cells were treated for 30 min with SAR405 (3 μM) before immunostaining for HA tag and total Rab10 or pT73-Rab10. Scale bar, 30 μm. **(B)** Left: percentage of cells with R1441G LRRK2⁺ endosomes. Middle and right: mean pT73-Rab10 or mean total Rab10 fluorescence intensity per cell. Statistical significance was calculated via unpaired, two-tailed t test with Bonferroni correction (n = 3 wells, >250 cells per well). Error bars: mean ± SEM. **p < 0.01; ***p < 0.001. **(C)** Representative sequential live cell images of stable T-REx HEK293 cells expressing GFP-tagged R1441G LRRK2 treated with SAR405 (3 μM). After 30 min, DMSO or MLi-2 (1 μM) was added to the cell media. Cells were imaged approximately every 5 min. Scale bar, 20 μm. **(D)** Quantification of the percentage of cells with LRRK2⁺ endosomes. Shaded areas: mean ± SEM (n = 7 fields of view per condition, >20 cells analyzed per field of view). **(E)** Model of positive feedback on endosomes. Red text: perturbations used in (A)–(D).

inhibition, we did not observe a significant decrease in LRRK2⁺ endosome formation in cells expressing these single or double Rab-binding mutants (**Figures A.5E-F**). Though, in untreated conditions, the Rab-binding mutations decreased the relatively small percentage of cells with R1441G LRRK2⁺ foci. It remains possible that under VPS34 inhibited conditions, weak binding

of Rabs to LRRK2 and/or additional Rab binding site(s)[35] are sufficient for positive feedback to initiate LRRK2$^+$ endosome formation.

2.3.5 Differential effects of GTPase-inactivating and kinase-activating mutations on LRRK2 localization and activity are consistent across a panel of mutants

Finally, to test the generality of our findings for G2019S and R1441G LRRK2, we expanded our study to include a total of 15 LRRK2 genotypes (WT LRRK2, 11 disease-associated LRRK2 mutants, protective variant R1398H LRRK2, kinase dead D2017A LRRK2, and GTP binding-deficient T1348N LRRK2) (**Figure 2.6A**). The selected mutations have a range of reported effects on LRRK2 activity, including modifications to the protein's GTPase and kinase functions (**Table A.1**). For each mutant, we quantified both the proportion of cells with LRRK2$^+$ endosomes and cellular p-Rab10 levels upon acute VPS34 inhibition (**Figures 2.6B-D**).

We note that p-Rab10 levels across LRRK2 mutants in control conditions were consistent with previously reported values (**Figure A.5G**),[8] and as before (**Figure 2.4B**), p-Rab10 levels were increased 3-fold across mutants in VPS34-inhibited vs. untreated conditions (**Figure A.5H**).

The strong correlation we observed between LRRK2$^+$ endosome formation and p-Rab10 levels suggested three groupings of mutants depending on whether LRRK2$^+$ endosome formation and p-Rab10 levels were well above, slightly above, or close to WT LRRK2 levels (groups 1–3; **Figure 2.6D**). Group 1 consists of disease-causing mutants that highly increase the formation of LRRK2$^+$ endosomes and lead to highly increased p-Rab10 levels (Y1699C, I2020T, R1441C/G/H, and N1437H). All group 1 mutants, with the exception of I2020T in the kinase domain, have reduced GTPase activity and increased GTP binding (**Table A.1**). Furthermore, all group 1 mutants are dephosphorylated at Ser935, which disrupts LRRK2 interaction with 14-3-3 proteins[7,22] (**Table A.1**).

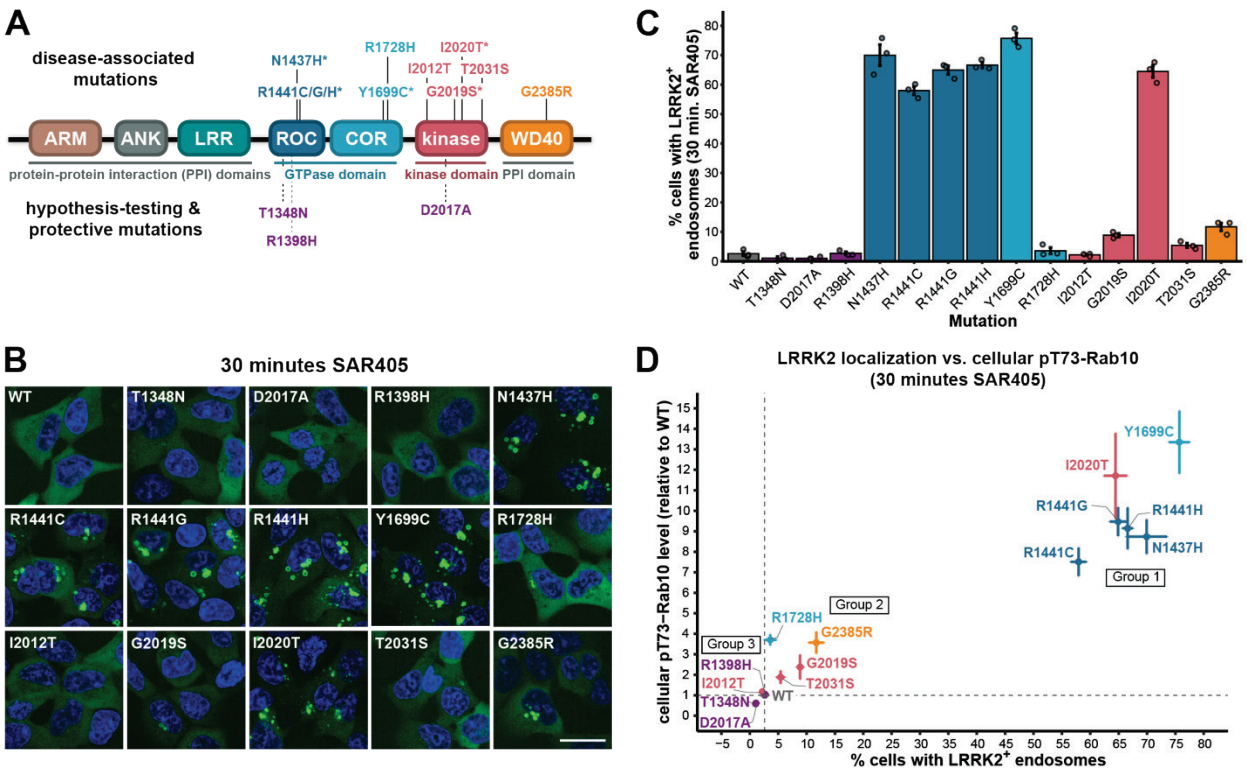

Figure 2.6: GTPase-inactivating LRRK2 mutants have higher LRRK2⁺ endosome formation and cellular p-Rab10 levels than kinase-activating mutants. (A) LRRK2 domain structure denoting the location of all mutations analyzed. Disease-associated mutations are on the top, while hypothesis-testing mutations (T1348N, D2017A) and a protective mutation (R1398H) are on the bottom. Asterisks indicate mutations that are causal for PD. **(B)** Representative live cell images of stable T-REx HEK293 cells expressing the indicated GFP-LRRK2 variants after 30 min treatment with SAR405 (3 μM). Scale bar, 25 μm. **(C)** Quantification of the percentage of cells with LRRK2⁺ endosomes observed via live imaging after 30 min. SAR405 treatment (3 μM) (n = 3 independent experiments, >500 cells analyzed per LRRK2 genotype in each experiment). **(D)** Scatterplot showing the percent of cells with LRRK2⁺ endosomes (using data from C) vs. cellular pT73-Rab10 levels after 30 min. SAR405 treatment (3 μM). pT73-Rab10 levels were quantified as the mean pT73-Rab10 fluorescence intensity per cell via immunofluorescence (n = 3 independent experiments, >550 cells analyzed per LRRK2 genotype in each experiment). Dashed lines indicate values for WT LRRK2. Group 1: Y1699C, I2020T, R1441C/G/H, N1437H. Group 2: G2385R, G2019S, T2031S, R1728H. Group 3: R1398H, I2012T, T1348N, D2017A. Error bars: mean ± SEM.

Group 2 contains disease-associated mutants that only moderately increase the formation of LRRK2⁺ endosomes and modestly increased p-Rab10 levels (R1728H, T2031S, G2019S, and G2385R). Overall, mutants in group 2 have increased *in vitro* kinase activity, though G2385R has conflicting reported activity (**Table A.1**).

Finally, group 3 is made up of mutants that have LRRK2^{+} endosome and p-Rab10 levels that are similar, or decreased, compared with WT LRRK2 (I2012T, R1398H, D2017A, and T1348N). I2012T (a putative disease allele with decreased kinase activity) and R1398H (a putative protective allele with increased GTPase activity and decreased GTP binding) behaved similarly to WT LRRK2. D2017A (kinase dead) and T1348N (no GTP binding) had minimal LRRK2^{+} endosomes and low p-Rab10 levels.

Across the panel of LRRK2 mutants, we found that GTPase-inactivating mutants consistently had stronger effects on LRRK2 membrane localization and Rab phosphorylation compared with kinase-activating LRRK2 mutants. Furthermore, as demonstrated by our results for group 3 mutants, decreases in LRRK2 GTP binding or kinase activity reduce LRRK2^{+} endosome formation to WT LRRK2 levels or lower. Overall, the connection between LRRK2 membrane localization and Rab phosphorylation provides an explanation for reported inconsistencies in relative p-Rab levels across mutants in cellular and *in vitro* assays, which cannot capture effects of LRRK2 localization (**Figure A.5l**).

2.4 Discussion

All PD-causing LRRK2 mutations lead to substrate hyperphosphorylation in cells, albeit to varying degrees. Here, we investigated mechanisms underlying how LRRK2 GTPase-inactivating mutations—which do not affect kinase activity *in vitro*— could lead to much higher substrate phosphorylation than kinase-activating mutations in cells. We found that GTPase-inactivating LRRK2 mutants have a higher propensity than kinase-activating mutants to be maintained on Rab-containing endosomal membranes, thereby allowing for greater levels of Rab phosphorylation.

Acute VPS34 inhibition enriches for a pool of enlarged, maturing endosomes by delaying subsequent maturation stages.[28,30,36] This enrichment allowed us to visualize strong recruitment

of LRRK2 to endosomes and detect mutant-dependent differences in Rab localization and phosphorylation. We speculate that VPS34 inhibition prolongs an endosomal stage at which LRRK2 signaling normally occurs at lower levels. Prior studies described WT LRRK2 signaling on endosomes and, in one case, demonstrated that WT LRRK2 could regulate VPS34-dependent endosomal maturation.[17,37–39] Interestingly, VPS34 depletion causes neuronal degeneration in mice by disrupting the endosomal system, and multiple risk loci for PD are related to phosphoinositide signaling.[40–42] LRRK2 was reported to aberrantly localize to enlarged endosomal structures in brain tissue from patients with dementia with Lewy bodies,[43] and alterations in early endosomal morphology and endocytic cargo processing have been found in brain tissue from patients with PD[44]; however, recent investigations have questioned the ability of current antibodies to detect LRRK2 in human tissue.[45] Future studies may seek to determine whether our findings have corollaries in brain tissue from patients with PD. Further, it would be interesting to explore whether VPS34 inhibition mirrors disease-relevant cellular states, such as aging-related changes in phosphoinositide pools.

The establishment and maintenance of LRRK2$^+$ endosomes in our system are consistent with a model of positive feedback operating on endosomal membranes (**Figure 2.5E**). First, LRRK2 associates with endosomes,[17,39] which occurs with higher probability under conditions of VPS34 inhibition. Second, phosphorylation of Rabs by LRRK2 inhibits Rab membrane disassociation, leading to accumulation of p-Rabs.[11,13,14] Third, LRRK2 can bind to p-Rabs, leading to membrane accumulation of LRRK2 through a feedforward pathway.[33] Together, LRRK2 and Rabs mutually and positively enhance the endosomal membrane localization of one another.[33] Consistent with a model of overall positive feedback, we found that enhancing Rab dephosphorylation (via PPM1H expression) and inhibiting the ability of LRRK2 to phosphorylate Rabs (via MLi-2 treatment) blocked LRRK2$^+$ endosome establishment and maintenance.[33] Important next steps in understanding this positive feedback circuit include

elucidating upstream regulators, detailing mechanisms of LRRK2 and Rab mutual reinforcement, and identifying other cell types and cellular contexts (e.g., the lysosome or Golgi) where such feedback operates.

This feedback model provides a framework in which to suggest mutant-specific mechanisms underlying differences in cellular p-Rab levels. For example, the kinase-activating mutants may have increased ability to perpetuate feedback through Rab phosphorylation (due to their increased intrinsic kinase activity),[4,8] while the GTPase-inactivating mutants may have increased probability to initiate feedback through increased initial membrane association (similar to WT LRRK2 in the GTP-bound state or through reduced 14-3-3 binding in the cytoplasm).[4,7,46] Consistent with this model, LRRK2 GTPase-inactivating mutants are recruited more efficiently to the Golgi by Rab29 than WT LRRK2,[16] and the mutant with the strongest membrane-association phenotype (Y1699C LRRK2; **Figure 2.6D**) has both decreased GTPase activity and increased *in vitro* kinase activity.[8,47,48] Ultimately, our data show that GTPase-inactivating mutants have much stronger net effects than kinase-activating mutants on this positive feedback as measured by increases in both $LRRK2^{+}$ endosomal mass and p-Rab10 levels. Thus, even without elevated intrinsic kinase activity, the observed kinase output of GTPase-inactivating mutants in cells can be higher than that of kinase-activating mutants. Further elucidation of this observation will be aided by quantitative parameterization of this feedback circuit in cells, including measured on-, off-, and feedback rates.

LRRK2 possesses additional layers of intramolecular regulation involving both kinase and GTPase activity not studied here. For example, LRRK2 exists both in monomer (primarily cytoplasmic) and dimer/oligomer (enriched at membranes) states.[46,49] The LRRK2 monomer-dimer cycle is thought to be regulated via GTP binding, and LRRK2 phosphorylates Rabs only in the active, dimeric/oligomeric state.[4,46,50,51] Furthermore, LRRK2 contains numerous autophosphorylation sites across domains with incompletely understood functions.[4,52,53] Future

studies may explore the role of autophosphorylation sites within the GTPase domain of LRRK2 in regulating LRRK2^{+} endosome formation.

We observed a qualitative but striking correlation of disease risk with the three LRRK2 mutant phenotypic groupings (defined by high, medium, and low levels of LRRK2^{+} endosomes and Rab phosphorylation; **Figure 2.6D**). All mutations in group 1 (largely GTPase-inactivating mutations) are causal for PD, with estimates of disease penetrance at age 80 being high for R1441C/G mutation carriers (>80%). In group 2 (largely kinase-activating mutations), G2019S is considered causative, albeit with a lower penetrance (25%–42.5%), and the remaining mutations modestly increase risk of disease. Finally, R1398H in group 3, which increases GTPase activity, is a protective variant for PD.[1,54–56] Thus, LRRK2 cellular localization, which is functionally connected to cellular Rab phosphorylation, may be a driver of downstream disease risk.

Our study provides a rationale for why disease-associated mutations across LRRK2 lead to differing degrees of substrate phosphorylation in cells. In cells expressing GTPase-inactivating mutants, both LRRK2 endosomal membrane localization and downstream Rab phosphorylation are strongly increased compared with kinase-activating mutants. It is encouraging that Rab dephosphorylation and LRRK2 kinase inhibition reversed aberrant localization of LRRK2 mutants on endosomal membranes, as LRRK2 kinase inhibition is currently being evaluated in clinical trials for PD.[57] Our results also suggest that strategies to promote the cytoplasmic localization of LRRK2, perhaps by modulating GTPase function or disrupting LRRK2 dimerization, could be valuable alternative methods to explore for LRRK2 PD treatment.

Limitations of the study

We note several limitations of our study. First, for the ease of detecting LRRK2 behavior and to facilitate live imaging of dynamic LRRK2 localization across LRRK2 mutants, many experiments in this study relied on exogenous expression of GFP-labeled LRRK2. The extent to which mutant LRRK2 localizes on endosomes in an endogenous context should be explored further to demonstrate physiological relevance. Second, we were unable to distinguish properties of individual LRRK2^{+} endosomes given the dynamic behavior of the LRRK2^{+} endosomes and the resolution of microscopy performed. Future studies may explore potential mutant- or cell-type-dependent differences in parameters such as the relative amounts of LRRK2, LRRK2 substrates (e.g., Rab10), or other proteins (e.g., Rab5A, Rab7) on individual LRRK2^{+} endosomes. Third, we did not explore the origin or ultimate fate of LRRK2^{+} endosomes in our system. Live imaging studies utilizing labeled endosomal proteins, including Rab5 and Rab7, along with labeled LRRK2 would be ideal for this purpose.

2.5 Methods

Cell lines

The Flp-in T-REx HEK293 system (Invitrogen) was utilized for both stable plasmid transfection as well as doxycycline-induced expression, as described previously.[7,22] Base T-REx media was DMEM supplemented with 10% FBS, 1% penicillin/streptomycin solution. Prior to transfection, the T-REx HEK293 host cell line was cultured in base T-REx media supplemented with 100 μg/mL Zeocin and 15 μg/mL Blasticidin. Upon stable integration of pcDNA5FRT/TO plasmids, T-REx HEK293 cell lines were maintained in base T-REx media supplemented with 50 μg/mL Hygromycin B and 15 μg/mL Blasticidin. Cells were incubated at 37˚C with 5% CO2. The wild-type and LRRK2 R1441C KI mouse embryonic fibroblasts (MEFs) were a generous gift generated by the laboratory of Dr. Dario Alessi (MRC-PPU at the University of Dundee). MEFs

were cultured in DMEM supplemented with 10% FBS, 1% penicillin/streptomycin solution, and non-essential amino acids. Cells were incubated at 37˚C with 5% CO2.

Antibody and reagent usage

The following primary antibodies were used at the indicated dilutions for immunofluorescence (IF) and Western blot (WB): rabbit anti-Rab10 (abcam, #ab237703, 1:500 for IF with T-REx HEK293 cells, 1:250 for IF with MEF cells, 1:1000 for WB), rabbit anti-Rab10 (phospho-T73) (abcam, #ab241060, 1:100 for IF with T-REx HEK293 cells, 1:250 for IF with MEF cells, 1:500 for WB), rabbit anti-Rab8A (Cell Signaling Technology, #6975, 1:100 for IF with T-REx HEK293 cells, 1:150 for IF with MEF cells, 1:750-1:1000 for WB), rabbit anti-Rab8A (phospho-T72) (abcam, ab230260, 1:1000 for WB), rabbit anti-Rab35 (ThermoFisher, #PA5-31674, 1:500 for IF, 1:1000 for WB), mouse anti-a-tubulin (Cell Signaling Technology, #3873, 1:2000 for IF), rabbit anti-a-tubulin (Cell Signaling Technology, #2125, 1:50 for IF), mouse anti-HA-tag (ThermoFisher, #26183, 1:500 for IF), mouse anti-Rab5A (Cell Signaling Technology, #46449, 1:200 for IF), rabbit anti-EEA1 (Cell Signaling Technology, #3288, 1:100 for IF), rabbit anti-Rab7 (Cell Signaling Technology, #9367, 1:100 for IF, 1:1000 for WB), rabbit anti-Rab7 (phospho-S72) (abcam, ab302494, 1:1000 for WB), rabbit anti-Rab11 (Cell Signaling Technology, #5589, 1:100 for IF), rabbit anti-GM130 (Cell Signaling Technology, #12480, 1:3200 for IF), rabbit anti-LC3A/B (Cell Signaling Technology, #12741, 1:200 for IF), rabbit anti-LAMP1 (Cell Signaling Technology, #9091, 1:300 for IF), mouse anti-LRRK2 (NeuroMab/AntibodiesInc, #75-253, 1:1000 for WB), rabbit anti-GFP (Cell Signaling Technology, #2956, 1:1000 for WB), mouse anti-GAPDH (Cell Signaling Technology, #97166, 1:1000 for WB). AlexaFluor secondary antibodies (ThermoFisher) were used in immunofluorescence assays, and IRDye secondary antibodies (LI-COR) were used in Western blots. We note from the abcam product page that the anti-Rab8A (phospho-T72) antibody cross-reacts with phosphorylated Rab3A, Rab10, Rab35 and Rab43.

With the exception of the initial microscopy-based survey of LRRK2 localization, DMSO was used at a final concentration of 0.1%. All other compounds were used at the indicated concentrations. We note that MLi-2 leads to Rab10 dephosphorylation within 10 minutes.[58] MLi-2 has been reported to cause LRRK2 dephosphorylation and enhanced microtubule association for some LRRK2 genotypes at later timepoints.[8,58,59]

Plasmids and site-directed mutagenesis

cDNA constructs pcDNA5FRT/TO-GFP-LRRK2 WT (DU113363), pcDNA5FrtTO-GFP-LRRK2 T1348N (DU34766), pcDNA5FrtTOGFP-LRRK2 R1441G (DU13388), and pcDNA5FrtTO-GFP-LRRK2 D2017A (DU13364) for expression of GFP-tagged, full-length LRRK2 were from Dr. Dario Alessi. Site-directed mutagenesis (SDM) was used to generate additional LRRK2 mutant plasmids. Some LRRK2 plasmids contained SNP S1647T, which was reverted to the consensus WT amino acid (S1647) via SDM prior to performing all experiments in this study with the exception of the initial microscopy screen (**Figure A.1A**). SDM was performed using the Q5 Site-Directed Mutagenesis Kit (NEB #E0554S) according to the manufacturer's directions. The NEBaseChanger web-based tool was used to generate appropriate primer sequences and annealing temperatures. For all plasmids generated via SDM, the entire LRRK2 insert was sequence-verified before use in experiments.

Additional plasmids utilized in this study: pcDNA5FRT/TO GFP (DU13156) was from Dr. Dario Alessi, pCMV5D-HA-PPM1H (DU62789), pCMV5D-HA-PPM1H H153D (DU62928), and pcDNA5-FRT/TO-GFP-LRRK1 (DU30382) were from the MRC PPU Reagents and Services facility, and pmCherry-2xFYVE was a gift from Harald Stenmark (Addgene plasmid #140050). Plasmids were verified by Sanger sequencing before use in experiments. All plasmids with DU numbers can be found on the University of Dundee MRC PPU website: https://mrcppureagents.dundee.ac.uk/.

DNA constructs were amplified in high efficiency NEB 5-alpha Competent E. coli (#C2987H) and purified using a QIAprep Spin Miniprep Kit (#27106) or QIAGEN Plasmid Plus Midi Kit (#12943).

Flp-in T-REx HEK293 cell line generation

Transfections of GFP-tagged LRRK2 or GFP-only control pcDNA5FRT/TO plasmids were performed using jetPRIME transfection reagent (Polyplus #101000027) in base T-REx media. Cells were co-transfected in 6-well culture plates at 60-80% confluency at a 9:1 ratio of pOG44 plasmid (Invitrogen #V6005-20) to pcDNA5FRT/TO plasmid of interest. Media was replaced four hours after transfection. 24 hours after transfection, cells were split into 10 cm dishes in base T-REx media. 48 hours after transfection, media was replaced with selection media (base T-REx media supplemented with 10 μg/mL Blasticidin and 100 μg/mL Hygromycin B). Transfected cells were selected for approximately two weeks to isolate cells that had successful plasmid integration into the FRT site. For experiments, expression of the indicated protein was induced using doxycycline (1 μg/mL).

Immunofluorescence for T-Rex HEK293 cells

T-REx HEK293 cells were seeded in 384-well PhenoPlates (PerkinElmer #6057302) manually coated with collagen I in T-REx base media supplemented with doxycycline (1 μg/mL). Plated cells were incubated for 48 hours before indicated drug treatment and immunofluorescence.

Cells were fixed with 4% paraformaldehyde for 15 minutes followed by three PBS washes at room temperature. Cells were then permeabilized for 10 minutes using 0.3% Triton X-100 in PBS and washed three times with PBS-T (0.1% Tween-20 in PBS) at room temperature. For conditions utilizing anti-LAMP1 or anti-LC3A/B antibodies, cells were alternatively fixed with ice-cold 100% methanol for 10 minutes at -20˚C and not subjected to a

permeabilization step. Cells were then blocked with 1% BSA in PBS-T for one hour at room temperature. Cells were incubated with primary antibodies in blocking buffer for 16-18 hours at 4˚C. After three PBS-T washes, cells were incubated with secondary antibodies in blocking buffer for one hour at room temperature followed by three PBS-T washes. Hoechst (Invitrogen #H3570) was added at a 1:1000 dilution for 10 minutes to one of the final PBS-T washes for nuclei staining. An anti-alpha-tubulin (mouse or rabbit) antibody was included when possible to aid in cell segmentation during image processing.

Microscopy was performed using a PerkinElmer Operetta CLS System with confocal spinning-disk mode. Cells were imaged with a 40x water objective and standard filter sets.

Immunofluorescence for MEF cells

MEFs were seeded in 384-well PhenoPlates (PerkinElmer #6057302) in standard growth media. Plated cells were incubated for 48 hours before indicated drug treatment and immunofluorescence.

Cells were fixed with 4% paraformaldehyde for 15 minutes at 37˚C followed by two washes with 0.5% Triton X-100 in PBS (PBS-T) at room temperature. Cells were then incubated in ice-cold methanol for 10 minutes at 4˚C followed by two washes with PBS-T at room temperature. Cells were incubated for 15 minutes with PBS-T at room temperature. Cells were then blocked with 0.5% BSA in PBS-T for one hour at room temperature. Cells were incubated with primary antibodies in blocking buffer for 16-18 hours at 4˚C. After three PBS-T washes, cells were incubated with secondary antibodies in PBS-T for one hour at room temperature followed by three PBS-T washes. Hoechst (Invitrogen #H3570) was added at a 1:1000 dilution for 10 minutes to one of the final washes for nuclei staining.

Microscopy was performed using a PerkinElmer Operetta CLS System with confocal spinning-disk mode. Cells were imaged with a 40x water objective and standard filter sets.

Live cell microscopy

T-REx HEK293 cells were seeded in 96-well PhenoPlates (PerkinElmer #6055302) manually coated with collagen I in T-REx base media supplemented with doxycycline (1 μg/mL). Plated cells were incubated for 48 hours before live imaging. To label nuclei, cells were incubated with Hoechst (Invitrogen #H3570) diluted 1:2000 in media for 10 minutes at 37˚C before washing two times with warm media.

Microscopy was performed with a PerkinElmer Operetta CLS System, utilizing the live cell chamber to maintain an environment of 37˚C and 5% CO2. Cells were imaged using confocal spinning-disk mode with a 40x water objective and standard filter sets. Prior to drug treatment, cells were imaged once to capture a pre-treatment state. Immediately following drug addition, cells were imaged at the indicated regular intervals for up to 60 minutes. For live imaging of MLi-2 treatment effects, imaging was briefly paused (<1 minute) to allow for MLi-2 addition after 30 minutes of imaging.

Initial survey of LRRK2 localization

T-REx HEK293 cells expressing GFP-tagged LRRK2 plasmids were treated using the following endo-lysosomal pathway-targeting compounds and conditions: DMSO (control; 0.2%, 2 hours), brefeldin A[60,61] (ER-Golgi transport inhibitor; 25 μM, 2 hours), docetaxel[62–64] (microtubule transport inhibitor; 2 μM, 2 hours), nocodazole[61,65,66] (microtubule transport inhibitor; 10 μM, 2 hours), rotenone[67,68] (mitophagy/mitochondrial function inhibitor; 1 μM, 1.5 hours), chloroquine[19,69] (autophagy/lysosomal function inhibitor; 30 μM, 2 hours), and SAR405[31,70,71] (endocytosis inhibitor; 2 μM, 2 hours).

Following compound treatment, cells were fixed with 4% paraformaldehyde and processed for microscopy analysis as described above.

Dextran endocytosis assay

T-REx HEK293 cells were plated for live cell microscopy and stained with Hoechst as described above. Cells were then incubated with 10 kDa CF640R-labeled dextran (100 μg/mL, Biotium #80115) for 15 minutes at 37˚C in the presence of DMSO or SAR405. After incubation, cells were washed five times with pre-warmed medium containing either DMSO or SAR405. Cells were then immediately imaged via live-cell microscopy every 10 minutes for one hour in the appropriate media containing DMSO or SAR405.

PPM1H and 2xFYVE transient transfections

T-REx HEK293 cells stably transfected with LRRK2 plasmids were seeded in 96-well PhenoPlates (PerkinElmer #6055302) manually coated with collagen I in T-REx base media. Cells were transfected the next day at 40-60% confluence using jetPRIME transfection reagent (Polyplus) at a 2:1 jetPRIME reagent to DNA ratio.

HA-PPM1H, HA-PPM1H H153D plasmids were transfected using 25 ng DNA. Media was replaced with T-REx base media supplemented with doxycycline (1μg/mL) four hours after transfection. After 24 hours, drug treatment and immunofluorescence was performed.

The pmCherry-2xFYVE plasmid was transfected using 20 ng DNA. Media was replaced with T-REx base media supplemented with doxycycline (1 μg/mL) four hours after transfection. After 48 hours, drug treatment and live imaging was performed.

Phos-tag SDS-PAGE and western blotting

Cell lysate preparation and Western blot methods were roughly based on a published protocol for LRRK2 immunoblotting.[72] T-REx HEK293 cells were plated in 6-well tissue culture plates in T-REx base media supplemented with doxycycline (1 μg/mL). After 48 hours, cells

were treated with the indicated compounds for 30 minutes before cell lysis for 30 minutes on ice.

For standard immunoblot analysis, the lysis buffer contained the following components: 50 mM Tris HCl pH 7.5, 1% Triton X-100, 0.27 M sucrose, 1 mM EGTA, 1 mM EDTA, 2 mM PMSF Protease Inhibitor (ThermoFisher), 1 μg/mL Microcystin-LR (Cayman Chemical #10007188), and 1.5X Halt Protease and Phosphatase Inhibitor Cocktail (ThermoFisher #78440). For Phos-tag SDS-PAGE analysis, the lysis buffer contained the following components: 50 mM Tris HCl pH 7.5, 1% Triton X-100, 0.27 M sucrose, 0.1% B-mercaptoethanol, 1 μg/mL Microcystin-LR (Cayman Chemical #10007188), and 1.5X Halt Protease and Phosphatase Inhibitor Cocktail (ThermoFisher #78440). Cell extracts were centrifuged at 16,500 x g for 15 minutes at 4˚C to clarify the lysate and protein concentrations were measured via BCA assay (Pierce).

The Bio-Rad Mini-PROTEAN Electrophoresis System was used for electrophoresis and transfer steps. For standard immunoblot analysis, cell extracts (15 μg) were resolved by SDS-PAGE using 4-15% TGX precast gels (Bio-Rad #4561086) with tris/glycine/SDS buffer. For Phos-tag SDS-PAGE analysis, cell extracts (15 μg) were resolved using SuperSep Phos-tag (50 μmol/L), 12.5% precast gels (Wako #4548995049865). When performing Phos-tag analysis, cell extracts were simultaneously resolved using 4-15% TGX precast gels to blot for total levels of the protein of interest and levels of a loading control protein (GAPDH). Phos-tag gels were washed 3 times with transfer buffer containing 10mM EDTA and 0.05% SDS followed by 1 wash with transfer buffer containing 0.05% SDS before transfer. All transfers were performed onto PVDF membranes for 2-3 hours on ice. Membranes were blocked with LI-COR blocking buffer for one hour at room temperature followed by incubation with primary antibodies diluted in blocking buffer overnight at 4˚C. Membranes were washed thoroughly with TBS-T (0.1% Tween-20 in TBS) before incubation with secondary antibodies (IRDye, LI-COR) diluted in

blocking buffer at room temperature for one hour. Membranes were washed in TBS-T before imaging with an Azure 600 imager (Azure Biosystems).

Image analysis and data processing

Maximum intensity projections obtained from three to four z-slices per field of view were used for analysis and for representative images. Representative images were processed identically across LRRK2 genotypes within each figure panel.

Image analysis methods used here have been previously described in detail.[73,74] All image analysis was done in MATLAB. In brief, background intensity was subtracted from maximum projection images to remove nonuniform background illumination using the NIH ImageJ rolling ball background subtraction algorithm. Individual cells in each image were then identified by an in-house watershed-based segmentation algorithm that utilizes nuclear and cytoplasmic markers to determine cell boundaries.[74] In each image channel for biomarkers of interest, numerous features were measured and extracted from each identified cell, including whole-cell morphology and intensity features as well as object-based morphology and intensity features.[74] The following single-cell features were utilized: total cell area, cytoplasmic area, nuclear area, area and intensity of marker objects in the cell, intensity of a marker in the cell (non-object based), and the Pearson correlation coefficient across image channels within the cytoplasm of the cell (non-object based). For markers of interest in which object-specific features were desired (LRRK2, Rab5A, and 2xFYVE), objects were identified as follows: First, foreground images were calculated for the channel of interest by applying a tophat filter and gaussian blur to reduce pixel noise.[75] An object mask was then calculated by applying a threshold value to the foreground image. The threshold value was determined for each cell by first calculating the median pixel intensity of the marker of interest in that individual cell (calculated from the original, unfiltered cell image). The final object threshold was then calculated as the median intensity raised to an exponent and multiplied by a constant. The

scaling values (exponent and constant multiplier) were held constant across all cells analyzed in all experiments for the given biomarker. The scaling values were empirically selected for each biomarker to allow effective object identification across a range of object and cytoplasm intensities.

Quality control was performed before final analysis. Poorly segmented cells were removed according to the following parameters: cytoplasmic to nuclear area ratio less than 0.5 or total cell area less than 2500 px^2 (~225 μm^2). For HA-PPM1H and HA-PPM1H H153D transient transfection experiments, unsuccessfully transfected cells had a mean cellular HA-tag fluorescence of less than 80 a.u. and were excluded from analysis.

‘‘Percent of cells with $LRRK2^+$ objects/endosomes’’ was calculated as the number of cells in which the total area of LRRK2 objects in the cell was greater than 40 px^2 (3.5 μm^2) divided by the total number of cells. (The minimum area threshold was determined empirically to minimize false positives due to artefacts or small cytoplasmic objects previously described for some LRRK2 mutants.[7,25]) Nevertheless, a small fraction of DMSO-treated cells had cytoplasmic objects that surpassed this threshold (see **Figures 2.2C and A.1E**).) The term ‘‘endosomes’’ was used instead of ‘‘objects’’ in plot labels where appropriate after determining the identity of VPS34 inhibition-induced $LRRK2^+$ endosomes.

A non-automated quantification method was used for Figures A.4B–D. For each marker of interest (Rab10, pT73-Rab10, and Rab8A), cells containing more than one enlarged, perinuclear vesicle positive for the marker of interest were counted (within 8 fields of view for 3 wells per experimental condition). The counted cells were expressed as a percentage of the total number of cells present in the well (at least 50 cells were analyzed per well). We note that the proportion of cells positive for Rab10 (**Figure A.4B**) or Rab8A (**Figure A.4D**) enlarged, perinuclear vesicles may have been underestimated due to obscurement of vesicular localization by the overall cytoplasmic signal of the proteins.

Statistical analysis and plotting

Statistical analyses and plotting were performed in R (version 4.0.3) using standard packages (ggplot2, stats, DescTools). For experiments with only two groups, one-tailed or two-tailed unpaired t-tests were performed with Bonferroni correction to adjust for multiple comparisons where appropriate. For experiments comparing three or more groups, a one-way ANOVA (analysis of variance) was used. If the ANOVA determined that there was a difference between the means of at least two of the treatment groups, a post hoc test was used. Dunnett's post hoc test was used when determining statistical significance for comparisons between individual experimental groups and a control group, while Tukey's post hoc test was used when determining statistical significance for comparisons between all individual treatment groups. Detailed information regarding replicates and statistical tests used is provided in each figure legend. Cartoons in the graphical abstract, Figures 2.5E, and A.2B were created with BioRender.com (academic subscription).

2.6 References

1. Alessi, D.R., and Sammler, E. (2018). LRRK2 kinase in Parkinson's disease. Science *360*, 36–37. https://doi.org/10.1126/science.aar5683.

2. Paisán-Ruíz, C., Jain, S., Evans, E.W., Gilks, W.P., Simón, J., van der Brug, M., López de Munain, A., Aparicio, S., Gil, A.M., Khan, N., et al. (2004). Cloning of the gene containing mutations that cause PARK8-linked Parkinson's disease. Neuron *44*, 595–600. https://doi.org/10.1016/j.neuron.2004.10.023.

3. Zimprich, A., Biskup, S., Leitner, P., Lichtner, P., Farrer, M., Lincoln, S., Kachergus, J., Hulihan, M., Uitti, R.J., Calne, D.B., et al. (2004). Mutations in LRRK2 cause autosomal-dominant parkinsonism with pleomorphic pathology. Neuron *44*, 601–607. https://doi.org/10.1016/j.neuron.2004.11.005.

4. Berwick, D.C., Heaton, G.R., Azeggagh, S., and Harvey, K. (2019). LRRK2 Biology from structure to dysfunction: research progresses, but the themes remain the same. Mol. Neurodegener. *14*, 49. https://doi.org/10.1186/s13024-019-0344-2.

5. Taylor, M., and Alessi, D.R. (2020). Advances in elucidating the function of leucine-rich repeat protein kinase-2 in normal cells and Parkinson's disease. Curr. Opin. Cell Biol. *63*, 102–113. https://doi.org/10.1016/j.ceb.2020.01.001.

6. Lake, J., Reed, X., Langston, R.G., Nalls, M.A., Gan-Or, Z., Cookson, M.R., Singleton, A.B., Blauwendraat, C., and Leonard, H.L.; International Parkinson's Disease Genomics Consortium IPDGC (2022). Coding and noncoding variation in LRRK2 and Parkinson's disease risk. Mov. Disord. *37*, 95–105. https://doi.org/10.1002/mds.28787.

7. Nichols, R.J., Dzamko, N., Morrice, N.A., Campbell, D.G., Deak, M., Ordureau, A., Macartney, T., Tong, Y., Shen, J., Prescott, A.R., and Alessi, D.R. (2010). 14-3-3 binding to

LRRK2 is disrupted by multiple Parkinson's disease-associated mutations and regulates cytoplasmic localization. Biochem. J. *430*, 393–404. https://doi.org/10.1042/bj20100483.

8. Kalogeropulou, A.F., Purlyte, E., Tonelli, F., Lange, S.M., Wightman, M., Prescott, A.R., Padmanabhan, S., Sammler, E., and Alessi, D.R. (2022). Impact of 100 LRRK2 variants linked to Parkinson's disease on kinase activity and microtubule binding. Biochem. J. *479*, 1759–1783. https://doi.org/10.1042/bcj20220161.

9. Greggio, E., and Cookson, M.R. (2009). Leucine-rich repeat kinase 2 mutations and Parkinson's disease: three questions. Asn Neuro *1*, e00002. https://doi.org/10.1042/an20090007.

10. Liao, J., Wu, C.-X., Burlak, C., Zhang, S., Sahm, H., Wang, M., Zhang, Z.Y., Vogel, K.W., Federici, M., Riddle, S.M., et al. (2014). Parkinson disease-associated mutation R1441H in LRRK2 prolongs the ''active state'' of its GTPase domain. Proc. Natl. Acad. Sci. USA *111*, 4055–4060. https://doi.org/10.1073/pnas.1323285111.

11. Steger, M., Tonelli, F., Ito, G., Davies, P., Trost, M., Vetter, M., Wachter, S., Lorentzen, E., Duddy, G., Wilson, S., et al. (2016). Phosphoproteomics reveals that Parkinson's disease kinase LRRK2 regulates a subset of Rab GTPases. Elife *5*, e12813. https://doi.org/10.7554/elife.12813.

12. Steger, M., Diez, F., Dhekne, H.S., Lis, P., Nirujogi, R.S., Karayel, O., Tonelli, F., Martinez, T.N., Lorentzen, E., Pfeffer, S.R., et al. (2017). Systematic proteomic analysis of LRRK2-mediated Rab GTPase phosphorylation establishes a connection to ciliogenesis. Elife *6*, e31012. https://doi.org/10.7554/elife.31012.

13. Pfeffer, S.R. (2018). LRRK2 and Rab GTPases. Biochem. Soc. Trans. *46*, 1707–1712. https://doi.org/10.1042/bst20180470.

14. Gomez, R.C., Wawro, P., Lis, P., Alessi, D.R., and Pfeffer, S.R. (2019). Membrane association but not identity is required for LRRK2 activation and phosphorylation of Rab GTPases. J. Cell Biol. *218*, 4157–4170. https://doi.org/10.1083/jcb.201902184.

15. Liu, Z., Bryant, N., Kumaran, R., Beilina, A., Abeliovich, A., Cookson, M.R., and West, A.B. (2018). LRRK2 phosphorylates membrane-bound Rabs and is activated by GTP-bound Rab7L1 to promote recruitment to the trans-Golgi network. Hum. Mol. Genet. *27*, 385–395. https://doi.org/10.1093/hmg/ddx410.

16. Purlyte, E., Dhekne, H.S., Sarhan, A.R., Gomez, R., Lis, P., Wightman, M., Martinez, T.N., Tonelli, F., Pfeffer, S.R., and Alessi, D.R. (2018). Rab29 activation of the Parkinson's disease-associated LRRK2 kinase. EMBO J. *37*, 1–18. https://doi.org/10.15252/embj.201798099.

17. Liu, Z., Xu, E., Zhao, H.T., Cole, T., and West, A.B. (2020). LRRK2 and Rab10 coordinate macropinocytosis to mediate immunological responses in phagocytes. EMBO J. *39*, e104862. https://doi.org/10.15252/embj.2020104862.

18. Bonet-Ponce, L., Beilina, A., Williamson, C.D., Lindberg, E., Kluss, J.H., Saez-Atienzar, S., Landeck, N., Kumaran, R., Mamais, A., Bleck, C.K.E., et al. (2020). LRRK2 mediates tubulation and vesicle sorting from lysosomes. Sci. Adv. *6*, eabb2454. https://doi.org/10.1126/sciadv.abb2454.

19. Eguchi, T., Kuwahara, T., Sakurai, M., Komori, T., Fujimoto, T., Ito, G., Yoshimura, S.I., Harada, A., Fukuda, M., Koike, M., and Iwatsubo, T. (2018). LRRK2 and its substrate Rab GTPases are sequentially targeted onto stressed lysosomes and maintain their homeostasis. Proc. Natl. Acad. Sci. USA *115*, E9115–E9124. https://doi.org/10.1073/pnas.1812196115.

20. Beilina, A., Rudenko, I.N., Kaganovich, A., Civiero, L., Chau, H., Kalia, S.K., Kalia, L.V., Lobbestael, E., Chia, R., Ndukwe, K., et al. (2014). Unbiased screen for interactors of leucine-

rich repeat kinase 2 supports a common pathway for sporadic and familial Parkinson disease. Proc. Natl. Acad. Sci. USA *111*, 2626–2631. https://doi.org/10.1073/pnas.1318306111.

21. Kluss, J.H., Beilina, A., Williamson, C.D., Lewis, P.A., Cookson, M.R., and Bonet-Ponce, L. (2022). Lysosomal positioning regulates Rab10 phosphorylation at LRRK2+ lysosomes. Proc. Natl. Acad. Sci. USA 119, e2205492119. https://doi.org/10.1073/pnas.2205492119.

22. Dzamko, N., Deak, M., Hentati, F., Reith, A.D., Prescott, A.R., Alessi, D.R., and Nichols, R.J. (2010). Inhibition of LRRK2 kinase activity leads to dephosphorylation of Ser910/Ser935, disruption of 14-3-3 binding and altered cytoplasmic localization. Biochem. J. *430*, 405–413. https://doi.org/10.1042/bj20100784.

23. Ogata, J., Hirao, K., Nishioka, K., Hayashida, A., Li, Y., Yoshino, H., Shimizu, S., Hattori, N., and Imai, Y. (2021). A novel LRRK2 variant p.G2294R in the WD40 domain identified in familial Parkinson's disease affects LRRK2 protein levels. Int. J. Mol. Sci. *22*, 3708. https://doi.org/10.3390/ijms22073708.

24. Reynolds, A., Doggett, E.A., Riddle, S.M., Lebakken, C.S., and Nichols, R.J. (2014). LRRK2 kinase activity and biology are not uniformly predicted by its autophosphorylation and cellular phosphorylation site status. Front. Mol. Neurosci. *7*, 54. https://doi.org/10.3389/fnmol.2014.00054.

25. Greggio, E., Jain, S., Kingsbury, A., Bandopadhyay, R., Lewis, P., Kaganovich, A., van der Brug, M.P., Beilina, A., Blackinton, J., Thomas, K.J., et al. (2006). Kinase activity is required for the toxic effects of mutant LRRK2/dardarin. Neurobiol. Dis. *23*, 329–341. https://doi.org/10.1016/j.nbd.2006.04.001.

26. Roosen, D.A., and Cookson, M.R. (2016). LRRK2 at the interface of autophagosomes, endosomes and lysosomes. Mol. Neurodegener. *11*, 73. https://doi.org/10.1186/s13024-016-0140-1.

27. Hur, E.-M., Jang, E.-H., Jeong, G.R., and Lee, B.D. (2019). LRRK2 and membrane trafficking: nexus of Parkinson's disease. BMB Rep. *52*, 533–539. https://doi.org/10.5483/bmbrep.2019.52.9.186.

28. Wallroth, A., and Haucke, V. (2018). Phosphoinositide conversion in endocytosis and the endolysosomal system. J. Biol. Chem. *293*, 1526–1535. https://doi.org/10.1074/jbc.r117.000629.

29. Gillooly, D.J., Morrow, I.C., Lindsay, M., Gould, R., Bryant, N.J., Gaullier,J.M., Parton, R.G., and Stenmark, H. (2000). Localization of phosphatidylinositol 3-phosphate in yeast and mammalian cells. EMBO J. *19*, 4577–4588. https://doi.org/10.1093/emboj/19.17.4577.

30. Marcelic, M., MahmutefendicLucin, H., Jurak Begonja, A., Blagojevic Zagorac, G., and Lucin, P. (2022). Early endosomal Vps34-derived phosphatidylinositol-3-phosphate is indispensable for the biogenesis of the endosomal recycling compartment. Cells *11*, 962. https://doi.org/10.3390/cells11060962.

31. Miranda, A.M., Lasiecka, Z.M., Xu, Y., Neufeld, J., Shahriar, S., Simoes, S., Chan, R.B., Oliveira, T.G., Small, S.A., and Di Paolo, G. (2018). Neuronal lysosomal dysfunction releases exosomes harboring APP C-terminal fragments and unique lipid signatures. Nat. Commun. *9*, 291. https://doi.org/10.1038/s41467-017-02533-w.

32. Malik, A.U., Karapetsas, A., Nirujogi, R.S., Mathea, S., Chatterjee, D., Pal, P., Lis, P., Taylor, M., Purlyte, E., Gourlay, R., et al. (2021). Deciphering the LRRK code: LRRK1 and LRRK2 phosphorylate distinct Rab proteins and are regulated by diverse mechanisms. Biochem. J. *478*, 553–578. https://doi.org/10.1042/bcj20200937.

33. Vides, E.G., Adhikari, A., Chiang, C.Y., Lis, P., Purlyte, E., Limouse, C., Shumate, J.L., Spínola-Lasso, E., Dhekne, H.S., Alessi, D.R., and Pfeffer, S.R. (2022). A feed-forward pathway

drives LRRK2 kinase membrane recruitment and activation. Elife *11*, e79771. https://doi.org/10.7554/elife.79771.

34. Berndsen, K., Lis, P., Yeshaw, W.M., Wawro, P.S., Nirujogi, R.S., Wightman, M., Macartney, T., Dorward, M., Knebel, A., Tonelli, F., et al. (2019). PPM1H phosphatase counteracts LRRK2 signaling by selectively dephosphorylating Rab proteins. Elife *8*, e50416. https://doi.org/10.7554/elife.50416.

35. Dhekne, H.S., Tonelli, F., Yeshaw, W.M., Chiang, C.Y., Limouse, C., Jaimon, E., Purlyte, E., Alessi, D.R., and Pfeffer, S.R. (2023). Genome-wide screen reveals Rab12 GTPase as a critical activator of pathogenic LRRK2 kinase. Preprint at bioRxiv. https://doi.org/10.1101/2023.02.17.529028.

36. Law, F., Seo, J.H., Wang, Z., DeLeon, J.L., Bolis, Y., Brown, A., Zong, W.X., Du, G., and Rocheleau, C.E. (2017). The VPS34 PI3K negatively regulates RAB-5 during endosome maturation. J. Cell Sci. *130*, 2007–2017. https://doi.org/10.1242/jcs.194746.

37. Bonet-Ponce, L., and Cookson, M.R. (2022). LRRK2 recruitment, activity, and function in organelles. FEBS J. *289*, 6871–6890. https://doi.org/10.1111/febs.16099.

38. Härtlova, A., Herbst, S., Peltier, J., Rodgers, A., Bilkei-Gorzo, O., Fearns, A., Dill, B.D., Lee, H., Flynn, R., Cowley, S.A., et al. (2018). LRRK2 is a negative regulator of Mycobacterium tuberculosis phagosome maturation in macrophages. EMBO J. *37*, e98694. https://doi.org/10.15252/embj.201798694.

39. Schreij, A.M.A., Chaineau, M., Ruan, W., Lin, S., Barker, P.A., Fon, E.A., and McPherson, P.S. (2015). LRRK2 localizes to endosomes and interacts with clathrin-light chains to limit Rac1 activation. EMBO Rep. *16*, 79–86. https://doi.org/10.15252/embr.201438714.

40. Raghu, P., Joseph, A., Krishnan, H., Singh, P., and Saha, S. (2019). Phosphoinositides: regulators of nervous system function in health and disease. Front. Mol. Neurosci. *12*, 208. https://doi.org/10.3389/fnmol.2019.00208.

41. Nakatsu, F., Messa, M., Nández, R., Czapla, H., Zou, Y., Strittmatter, S.M., and De Camilli, P. (2015). Sac2/INPP5F is an inositol 4-phosphatase that functions in the endocytic pathway. J. Cell Biol. *209*, 85–95. https://doi.org/10.1083/jcb.201409064.

42. Krebs, C.E., Karkheiran, S., Powell, J.C., Cao, M., Makarov, V., Darvish, H., Di Paolo, G., Walker, R.H., Shahidi, G.A., Buxbaum, J.D., et al. (2013). The Sac1 domain of SYNJ1 identified mutated in a family with early-onset progressive parkinsonism with generalized seizures. Hum. Mutat. *34*, 1200–1207. https://doi.org/10.1002/humu.22372.

43. Higashi, S., Moore, D.J., Yamamoto, R., Minegishi, M., Sato, K., Togo, T., Katsuse, O., Uchikado, H., Furukawa, Y., Hino, H., et al. (2009). Abnormal localization of leucine-rich repeat kinase 2 to the endosomal-lysosomal compartment in Lewy body disease. J. Neuropathol. Exp. Neurol. *68*, 994–1005. https://doi.org/10.1097/nen.0b013e3181b44ed8.

44. Rocha, E.M., De Miranda, B.R., Castro, S., Drolet, R., Hatcher, N.G., Yao, L., Smith, S.M., Keeney, M.T., Di Maio, R., Kofler, J., et al. (2020). LRRK2 inhibition prevents endolysosomal deficits seen in human Parkinson's disease. Neurobiol. Dis. *134*, 104626. https://doi.org/10.1016/j.nbd.2019.104626.

45. Fernández, B., Chittoor-Vinod, V.G., Kluss, J.H., Kelly, K., Bryant, N., Nguyen, A.P.T., Bukhari, S.A., Smith, N., Lara Ordóñez, A.J., Fdez, E., et al. (2022). Evaluation of current methods to detect cellular leucine-rich repeat kinase 2 (LRRK2) kinase activity. J Parkinsons Dis. *12*, 1423– 1447. https://doi.org/10.3233/jpd-213128.

46. Berger, Z., Smith, K.A., and LaVoie, M.J. (2010). Membrane localization of LRRK2 is associated with increased formation of the highly active LRRK2 dimer and changes in its phosphorylation. Biochemistry *49*, 5511–5523. https://doi.org/10.1021/bi100157u.

47. Biosa, A., Trancikova, A., Civiero, L., Glauser, L., Bubacco, L., Greggio, E.,and Moore, D.J. (2013). GTPase activity regulates kinase activity and cellular phenotypes of Parkinson's disease-associated LRRK2. Hum.Mol. Genet. *22*, 1140–1156. https://doi.org/10.1093/hmg/dds522.

48. Lobbestael, E., Baekelandt, V., and Taymans, J.-M. (2012). Phosphorylation of LRRK2: from kinase to substrate. Biochem. Soc. Trans. *40*, 1102–1110. https://doi.org/10.1042/bst20120128.

49. Zhu, H., Tonelli, F., Alessi, D.R., and Sun, J. (2022). Structural basis of human LRRK2 membrane recruitment and activation. Preprint at bioRxiv. https://doi.org/10.1101/2022.04.26.489605.

50. Park, Y., Liao, J., and Hoang, Q.Q. (2022). Roc, the G-domain of the Parkinson's disease-associated protein LRRK2. Trends Biochem. Sci. *47*,1038–1047. https://doi.org/10.1016/j.tibs.2022.06.009.

51. Wu, C.-X., Liao, J., Park, Y., Reed, X., Engel, V.A., Hoang, N.C., Takagi, Y.,Johnson, S.M., Wang, M., Federici, M., et al. (2019). Parkinson's disease-associated mutations in the GTPase domain of LRRK2 impair its nucleotide-dependent conformational dynamics. J. Biol. Chem. *294*, 5907–5913. https://doi.org/10.1074/jbc.ra119.007631.

52. Deyaert, E., Wauters, L., Guaitoli, G., Konijnenberg, A., Leemans, M., Terheyden, S., Petrovic, A., Gallardo, R., Nederveen-Schippers, L.M., Athanasopoulos, P.S., et al. (2017). A homologue of the Parkinson's disease-associated protein LRRK2 undergoes a monomer-dimer

transition during GTP turnover. Nat. Commun. *8*, 1008. https://doi.org/10.1038/s41467-017-01103-4.

53. Marchand, A., Drouyer, M., Sarchione, A., Chartier-Harlin, M.-C., and Taymans, J.-M. (2020). LRRK2 phosphorylation, more than an epiphenomenon. Front. Neurosci. *14*, 527. https://doi.org/10.3389/fnins.2020.00527.

54. Haugarvoll, K., Rademakers, R., Kachergus, J.M., Nuytemans, K., Ross,O.A., Gibson, J.M., Tan, E.-K., Gaig, C., Tolosa, E., Goldwurm, S., et al.(2008). Lrrk2 R1441C parkinsonism is clinically similar to sporadic Parkinson disease. Neurology *70*, 1456–1460. https://doi.org/10.1212/01.wnl.0000304044.22253.03.

55. Ruiz-Martínez, J., Gorostidi, A., Ibañez, B., Alzualde, A., Otaegui, D., Moreno, F., López de Munain, A., Bergareche, A., Gómez-Esteban, J.C., and Martí Massó, J.F. (2010). Penetrance in Parkinson's disease related to the LRRK2 R1441G mutation in the Basque country (Spain). Mov. Disord. *25*, 2340–2345. https://doi.org/10.1002/mds.23278.

56. Lee, A.J., Wang, Y., Alcalay, R.N., Mejia-Santana, H., Saunders-Pullman, R., Bressman, S., Corvol, J.C., Brice, A., Lesage, S., Mangone, G., et al. (2017). Penetrance estimate of LRRK2 p.G2019S mutation in individuals of non-Ashkenazi Jewish ancestry: LRRK2 Mutation in Non-Ashkenazi Jewish Ancestry. Mov. Disord. *32*, 1432–1438. https://doi.org/10.1002/mds.27059.

57. Jennings, D., Huntwork-Rodriguez, S., Henry, A.G., Sasaki, J.C., Meisner, R., Diaz, D., Solanoy, H., Wang, X., Negrou, E., Bondar, V.V., et al. (2022). Preclinical and clinical evaluation of the LRRK2 inhibitor DNL201 for Parkinson's disease. Sci. Transl. Med. *14*, eabj2658. https://doi.org/10.1126/scitranslmed.abj2658.

58. Ito, G., Katsemonova, K., Tonelli, F., Lis, P., Baptista, M.A.S., Shpiro, N., Duddy, G., Wilson, S., Ho, P.W.-L., Ho, S.-L., et al. (2016). Phos-tag analysis of Rab10 phosphorylation by LRRK2:

a powerful assay for assessing kinase function and inhibitors. Biochem. J. *473*, 2671–2685. https://doi.org/10.1042/bcj20160557.

59. Schmidt, S.H., Weng, J.-H., Aoto, P.C., Boassa, D., Mathea, S., Silletti, S., Hu, J., Wallbott, M., Komives, E.A., Knapp, S., et al. (2021). Conformation and dynamics of the kinase domain drive subcellular location and activation of LRRK2. Proc. Natl. Acad. Sci. USA *118*, e2100844118. https://doi.org/10.1073/pnas.2100844118.

60. Fujiwara, T., Oda, K., Yokota, S., Takatsuki, A., and Ikehara, Y. (1988). Brefeldin A causes disassembly of the Golgi complex and accumulation of secretory proteins in the endoplasmic reticulum. J. Biol. Chem. *263*, 18545–18552. https://doi.org/10.1016/s0021-9258(19)81393-5.

61. Martinez, H., Garcı´a, I.A., Sampieri, L., and Alvarez, C. (2016). Spatial-temporal study of Rab1b dynamics and function at the ER-golgi interface. PLoS One *11*, e0160838. https://doi.org/10.1371/journal.pone.0160838.

62. Kett, L.R., Boassa, D., Ho, C.C.-Y., Rideout, H.J., Hu, J., Terada, M., Ellisman, M., and Dauer, W.T. (2012). LRRK2 Parkinson disease mutations enhance its microtubule association. Hum. Mol. Genet. *21*, 890–899. https://doi.org/10.1093/hmg/ddr526.

63. Watanabe, R., Buschauer, R., Bo¨hning, J., Audagnotto, M., Lasker, K., Lu,T.-W., Boassa, D., Taylor, S., and Villa, E. (2020). The in situ structure of Parkinson's disease-linked LRRK2. Cell *182*, 1508–1518.e16. https://doi.org/10.1016/j.cell.2020.08.004.

64. Wu, X., Sooman, L., Lennartsson, J., Bergstro¨m, S., Bergqvist, M., Gullbo,J., and Ekman, S. (2013). Microtubule inhibition causes epidermal growth factor receptor inactivation in oesophageal cancer cells. Int. J. Oncol. *42*, 297–304. https://doi.org/10.3892/ijo.2012.1710.

65. Etoh, K., and Fukuda, M. (2019). Rab10 regulates tubular endosome formation through KIF13A and KIF13B motors. J. Cell Sci. *132*, jcs226977. https://doi.org/10.1242/jcs.226977.

66. Xie, R., Nguyen, S., McKeehan, W.L., and Liu, L. (2010). Acetylated micro-tubules are required for fusion of autophagosomes with lysosomes. BMC Cell Biol. *11*, 89. https://doi.org/10.1186/1471-2121-11-89.

67. Di Maio, R., Hoffman, E.K., Rocha, E.M., Keeney, M.T., Sanders, L.H., DeMiranda, B.R., Zharikov, A., Van Laar, A., Stepan, A.F., Lanz, T.A., et al.(2018). LRRK2 activation in idiopathic Parkinson's disease. Sci. Transl. Med. *10*, eaar5429. https://doi.org/10.1126/scitranslmed.aar5429.

68. Peng, K., Xiao, J., Yang, L., Ye, F., Cao, J., and Sai, Y. (2019). Mutual antagonism of PINK1/parkin and PGC-1acontributes to maintenance of mitochondrial homeostasis in rotenone-induced neurotoxicity. Neurotox. Res. *35*, 331–343. https://doi.org/10.1007/s12640-018-9957-4.

69. Mauthe,M.,Orhon,I.,Rocchi,C.,Zhou,X.,Luhr,M.,Hijlkema,K.-J.,Coppes,R.P., Engedal, N., Mari, M., and Reggiori, F. (2018). Chloroquine inhibits autophagic flux by decreasing autophagosome-lysosome fusion. Autophagy *14*, 1435–1455. https://doi.org/10.1080/15548627.2018.1474314.

70. Tan, K.W., Nähse, V., Campsteijn, C., Brech, A., Schink, K.O., and Stenmark, H. (2021). JIP4 is recruited by the phosphoinositide-binding protein Phafin2 to promote recycling tubules on macropinosomes. J. Cell Sci. *134*, jcs258495. https://doi.org/10.1242/jcs.258495.

71. Ronan, B., Flamand, O., Vescovi, L., Dureuil, C., Durand, L., Fassy, F., Bachelot, M.-F., Lamberton, A., Mathieu, M., Bertrand, T., et al. (2014). A highly potent and selective Vps34 inhibitor alters vesicle trafficking and autophagy. Nat. Chem. Biol. *10*, 1013–1019. https://doi.org/10.1038/nchembio.1681.

72. Tonelli, F., and Alessi, D. (2021). Quantitative immunoblotting analysis of LRRK2 signalling pathway v1. https://doi.org/10.17504/protocols.io.bsgrnbv6.

73. Kang, J., Hsu, C.-H., Wu, Q., Liu, S., Coster, A.D., Posner, B.A., Altschuler, S.J., and Wu, L.F. (2016). Improving drug discovery with high-content phenotypic screens by systematic selection of reporter cell lines. Nat. Biotechnol. *34*, 70–77. https://doi.org/10.1038/nbt.3419.

74. Loo, L.-H., Wu, L.F., and Altschuler, S.J. (2007). Image-based multivariate profiling of drug responses from single cells. Nat. Methods *4*, 445–453. https://doi.org/10.1038/nmeth1032.

75. Greene, C. (2022). filt2 2D geospatial data filter. MATLAB Central File Exchange. https://www.mathworks.com/matlabcentral/fileexchange/61003filt2-2d-geospatial-data-filter.

Appendix A:

Supplemental Material for Chapter 2

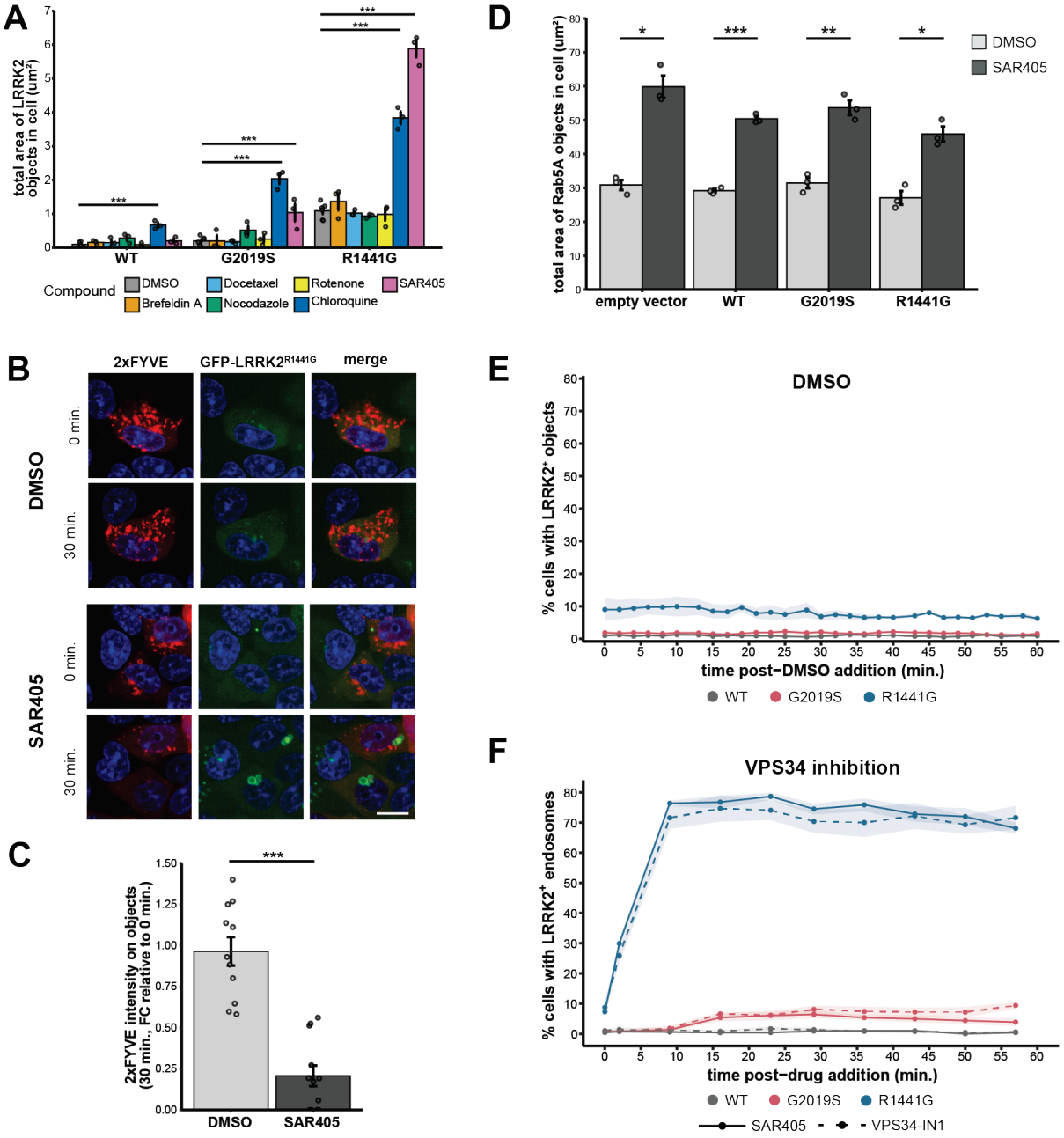

Figure A.1: VPS34 inhibition reveals mutant-specific LRRK2 localization pattern. (A) Quantification of the mean total area of LRRK2 localized on objects per cell. Each point represents the mean of single-cell measurements for all imaged cells within a well. Statistical significance was calculated via one-way ANOVA followed by Dunnett's post hoc test (n = 6 wells for DMSO, 3 wells for all other compounds, >65 cells per well). **(B)** Representative images of live stable T-REx HEK293 cells expressing GFP-tagged R1441G LRRK2 and transiently transfected with a plasmid encoding the PI3P probe mCherry-2xFYVE. Cells were treated with DMSO or SAR405 (3 μM) before live imaging. SAR405 treatment reduced mCherry-2xFYVE signal concomitant with an increase in R1441G LRRK2 endosomal membrane localization. Scale bar, 15 μm. **(C)** Quantification of mCherry-2xFYVE intensity on objects as a percent of total cellular mCherry-2xFYVE intensity in cells expressing GFP-R1441G LRRK2. Data shown as fold change (FC) in 2xFYVE intensity on objects 30 min after compound treatment relative to 2xFYVE intensity on objects in the same cell prior to treatment. Statistical significance was calculated via

(caption continued from previous page) unpaired, two-tailed t test (n = 11 cells DMSO, 12 cells SAR405). **(D)** Quantification of total area of $Rab5A^+$ objects after 30 min treatment with DMSO or SAR405 (3 μM). Each point represents the mean of single-cell measurements for all imaged cells within a well. Statistical significance was calculated via unpaired, two-tailed t tests with Bonferroni correction (n = 3 wells, >90 cells per well). A-D: Error bars: mean +/- SEM. * indicates p values <0.05; ** indicates p values < 0.01; *** indicates p values < 0.001. **(E)** Stable T-REx HEK293 cells expressing the indicated GFP-tagged LRRK2 variants were treated with DMSO and analyzed via live-cell imaging. Cells were imaged approximately every 2 min. Quantification of percent of cells with LRRK2 localized on objects (n = 4 independent experiments, >200 cells analyzed per LRRK2 genotype in each experiment). **(F)** Stable T-REx HEK293 cells expressing the indicated GFP-tagged LRRK2 variants were treated with SAR405 (3 μM) or VPS34-IN1 (3 μM) and analyzed via live-cell imaging. Cells were imaged approximately every 7 min. Quantification of percent of cells with $LRRK2^+$ endosomes (n = 8 fields of view per condition, >20 cells analyzed per field of view). E-F: Shaded areas: mean +/- SEM.

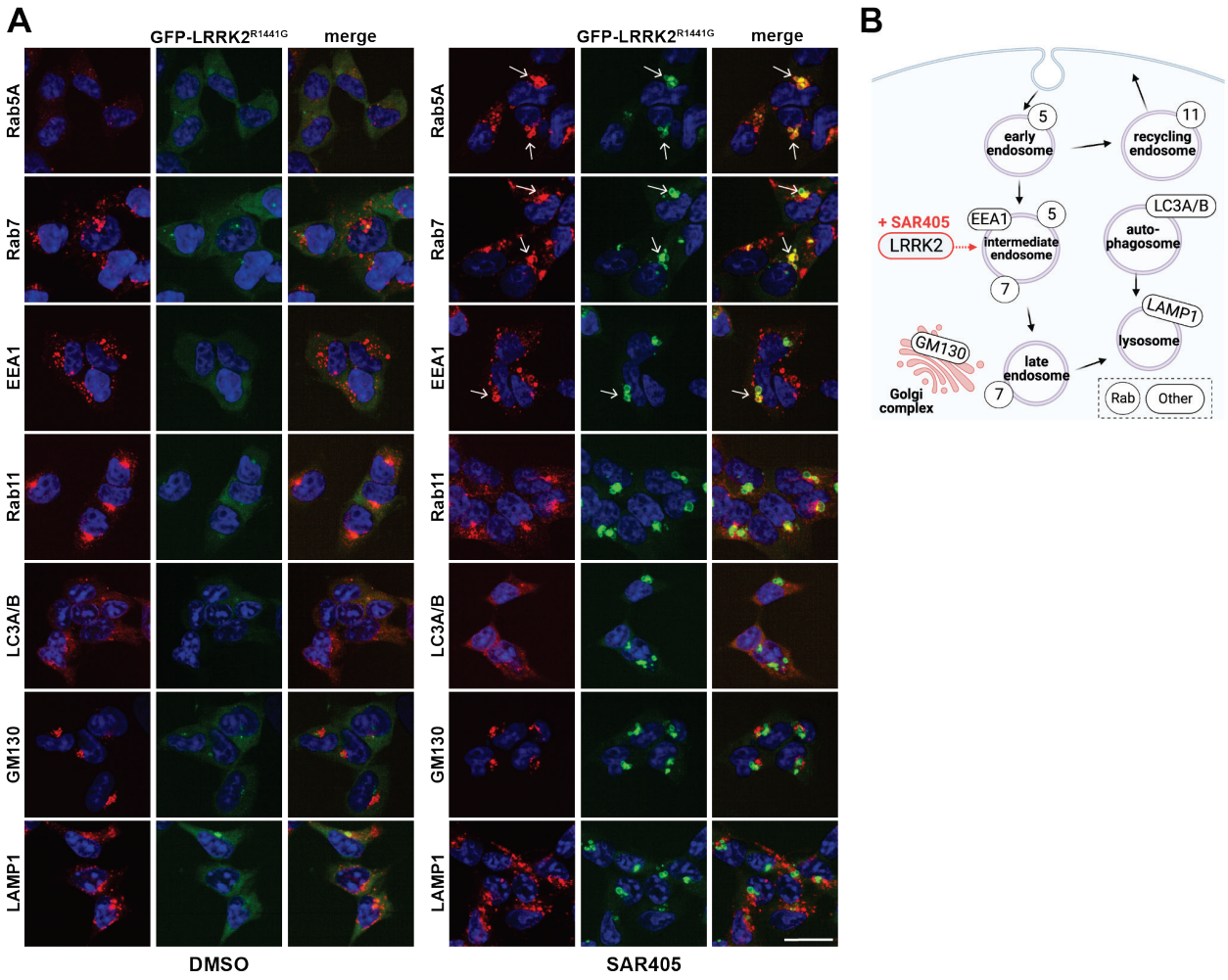

Figure A.2: LRRK2 co-localizes with early and late endosomal markers upon VPS34 inhibition. (A) Representative images demonstrating co-localization of GFP-tagged R1441G LRRK2 with endo-lysosomal biomarkers. Cells were treated for 30 min with DMSO or SAR405 (3 μM) before immunostaining for indicated proteins. Arrows indicate strong co-localization of R1441G LRRK2^{+} vesicles with Rab5A, Rab7, and EEA1 in the SAR405 condition. Scale bar, 25 μm. **(B)** Simplified cartoon indicating the identity of vesicles or organelles labeled with the endo-lysosomal biomarkers[1-3]. SAR405 treatment reveals LRRK2 co-localization with markers of intermediate, maturing endosomes.

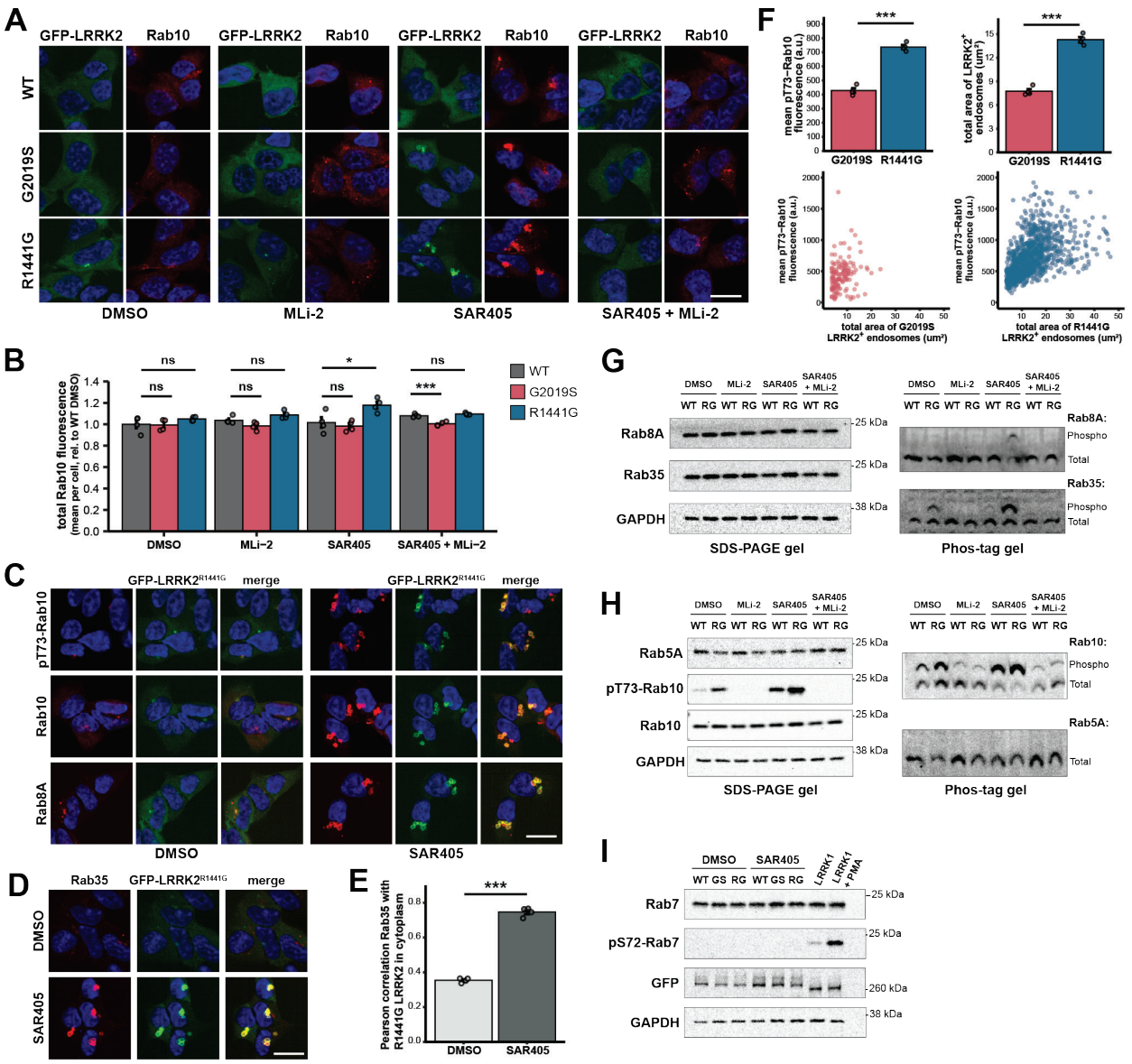

Figure A.3: Additional analysis of VPS34 inhibition effects on LRRK2-mediated Rab phosphorylation. (A) Representative images of stable T-REx HEK293 cells expressing GFP-tagged LRRK2 variants after 30 min drug treatment and immunostaining for total Rab10. MLi-2: 1 μM, SAR405: 3 μM. **(B)** Quantification of mean total Rab10 fluorescence intensity per cell displayed as fold change relative to DMSO-treated cells expressing WT LRRK2. Each point represents the mean of single-cell measurements for all imaged cells within a well. Statistical significance was calculated via one-way ANOVA followed by Dunnett's post hoc test (n = 4 wells, >250 cells per well). **(C)** Representative images demonstrating strong co-localization of GFP-tagged R1441G LRRK2 with total and phospho-Rab proteins upon VPS34 inhibition. Cells were treated for 30 min with DMSO or SAR405 (3 μM) before immunostaining for Rab10, pT73-Rab10, or Rab8A. **(D)** Representative images demonstrating strong co-localization of GFP-tagged R1441G LRRK2 with total Rab35 upon VPS34 inhibition. Cells were treated for 30 min with DMSO or SAR405 (3 μM) before immunostaining for Rab35. **(E)** Co-localization analysis of GFP-tagged R1441G LRRK2 with Rab35 after 30 min treatment with DMSO or SAR405 (3 μM). Each point represents the mean of single-cell measurements for all imaged cells within a well. Statistical significance was calculated via unpaired, one-tailed t test (n = 4 wells, >150 cells per well). **(F)** Top:

(caption continued from previous page) Quantification of the mean pT73-Rab10 fluorescence or total area of LRRK2^{+} endosomes per cell for SAR405-treated cells in Fig. 3B containing LRRK2^{+} endosomes. Statistical significance was calculated via unpaired, two-tailed t tests with Bonferroni correction (n = 4 wells, >25 cells G2019S and >220 cells R1441G analyzed per well). Bottom: Scatter plots of mean pT73-Rab10 fluorescence vs. total area of LRRK2^{+} endosomes per cell for pooled single cells summarized in above barplots. (n = 144 cells G2019S, 1051 cells R1441G). **(G)** Stable T-REx HEK293 cells expressing GFP-tagged LRRK2 variants were treated for 30 min with the indicated compounds. Samples were subjected to either standard SDS-PAGE (left) or phos-tag electrophoresis (right) followed by immunoblotting for Rab8A and Rab35 phosphorylation analysis. MLi-2: 1 μM, SAR405: 3 μM. **(H)** Stable T-REx HEK293 cells expressing GFP-tagged LRRK2 variants were treated for 30 min with the indicated compounds. Samples were subjected to either standard SDS-PAGE (left) or phos-tag electrophoresis (right) followed by immunoblotting for Rab5A and Rab10 (positive control) phosphorylation analysis. MLi-2: 1 μM, SAR405: 3 μM. **(I)** Western blot for total and phosphorylated Rab7 after 30 min treatment with the indicated compounds. As a positive control, lysates from stable T-REx HEK293 cells expressing GFP-LRRK1 were included in this analysis. LRRK1 is known to phosphorylate Rab7 at the S72 site, and this effect is enhanced by treatment with phorbol 12-myristate 13-acetate (PMA). SAR405: 3 μM, PMA: 100 ng/mL. GS = G2019S, RG = R1441G. Scale bars, 20 μm. Error bars: mean +/- SEM. * indicates p values < 0.05; *** indicates p values < 0.001.

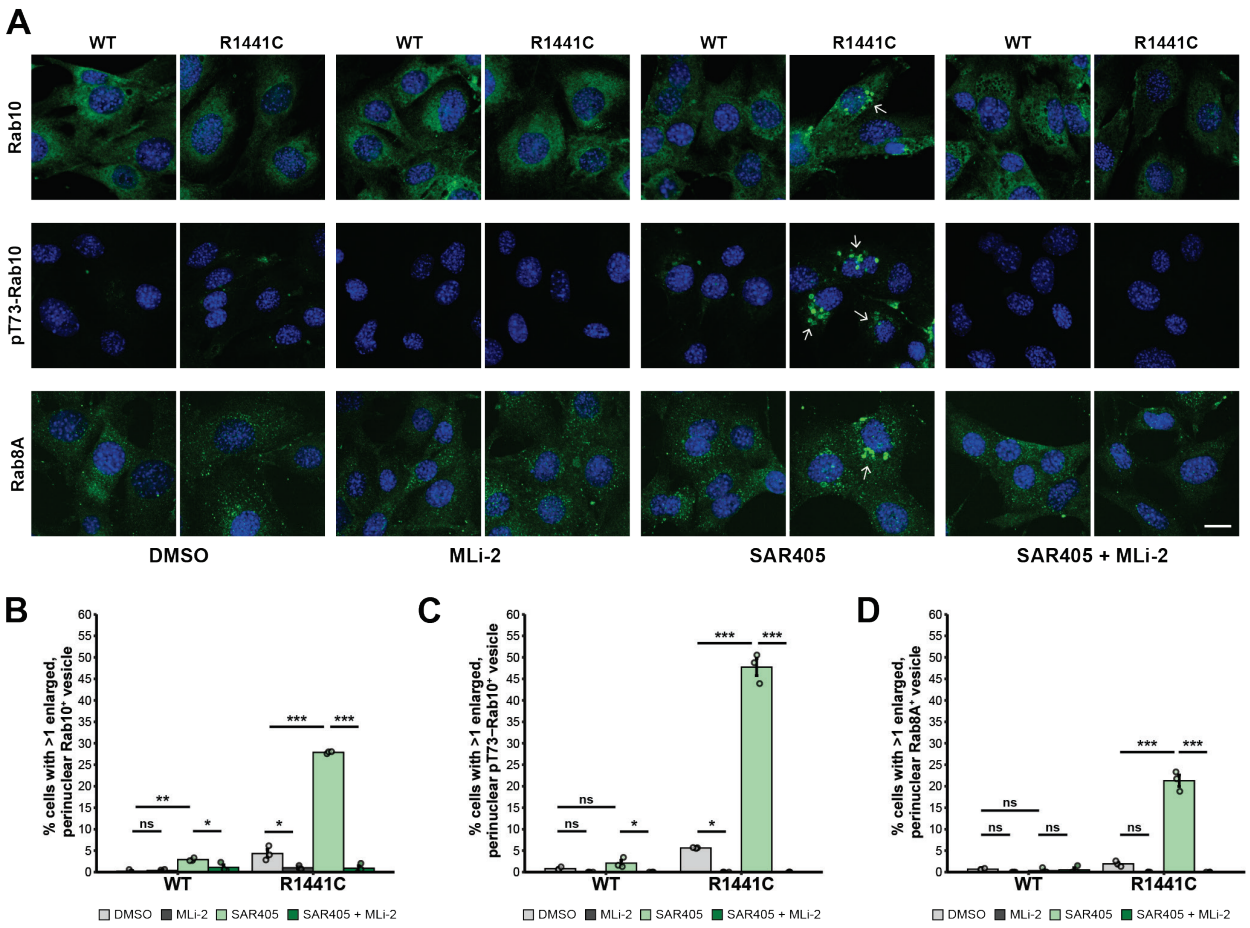

Figure A.4: VPS34 inhibition increases the proportion of R1441C MEFs containing Rab10^{+}, pT73-Rab10^{+}, and Rab8A^{+} perinuclear vesicles. (A) Representative images of WT and R1441C mouse embryonic fibroblasts (MEFs) after 2 hr drug treatment and immunostaining for total Rab10, pT73-Rab10, or total Rab8A. Arrows indicate cells with enlarged, perinuclear vesicles positive for Rab10, pT73-Rab10, or Rab8A in the SAR405 condition. Scale bar, 20 μm. **(B)** Quantification of the percent of cells with at least one enlarged, perinuclear vesicle positive for total Rab10 after 2 hr treatment with the indicated compounds. **(C)** Quantification of the percent of cells with at least one enlarged, perinuclear vesicle positive for pT73-Rab10 after 2 hr treatment with the indicated compounds. **(D)** Quantification of the percent of cells with at least one enlarged, perinuclear vesicle positive for total Rab8A after 2 hr treatment with the indicated compounds. A-D: MLi-2: 0.5 μM, SAR405: 10 μM. B-D: Statistical significance was calculated via one-way ANOVA followed by Tukey's post hoc test (n = 3 wells, >50 cells counted per well).

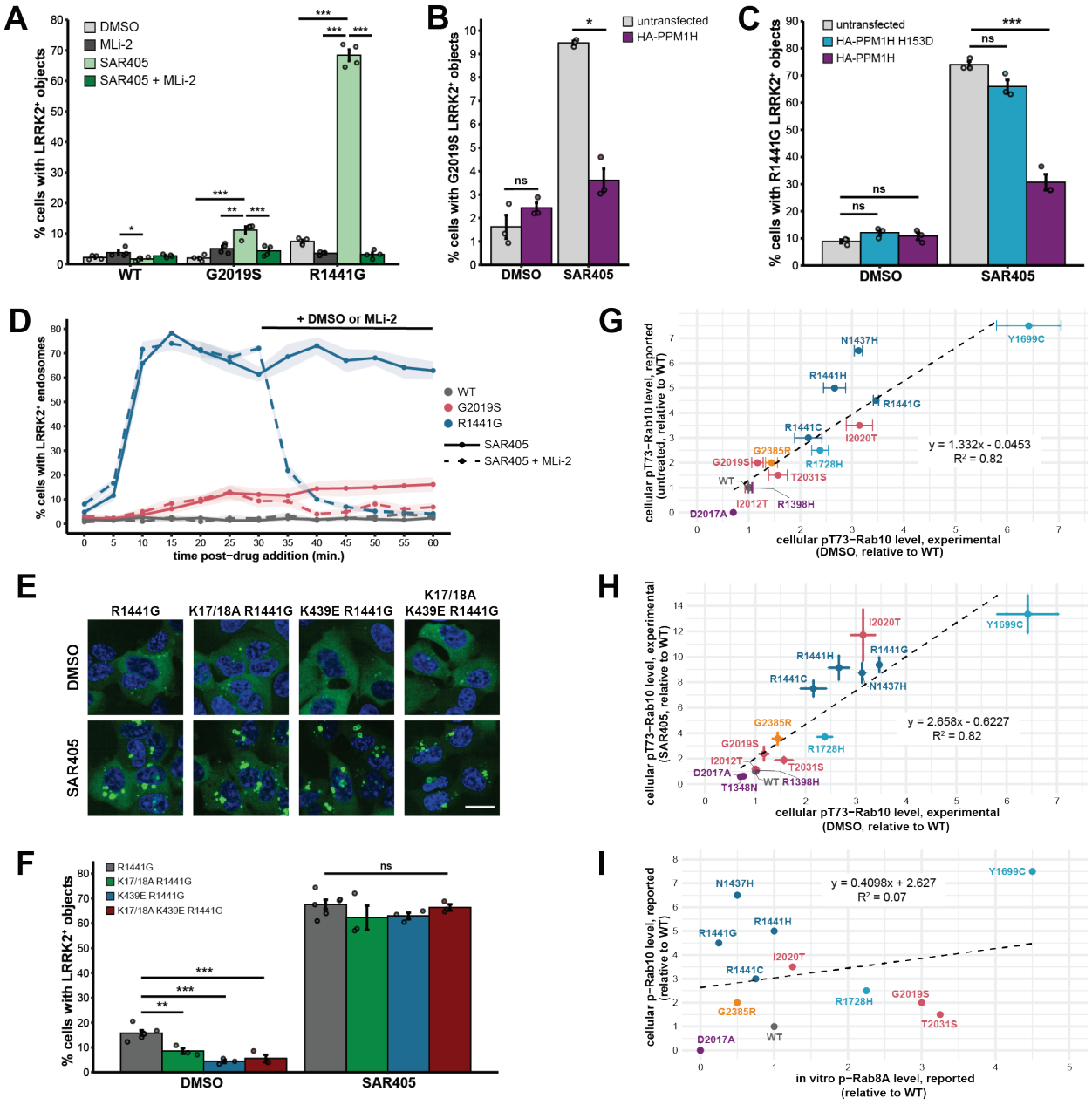

Figure A.5: Additional analysis of LRRK2⁺ endosome feedback mechanisms and trends across LRRK2 mutant panel. (A) Stable T-REx HEK293 cells expressing GFP-LRRK2 variants were treated for 30 min with the indicated compounds before fixation and quantification of the percent of cells with LRRK2⁺ endosomes. MLi-2: 1 μM, SAR405: 3 μM. Statistical significance was calculated via one-way ANOVA followed by Tukey's post hoc test (n = 4 wells, >200 cells per well). Unlabeled comparisons were not significant. **(B)** Stable T-REx HEK293 cells expressing GFP-tagged G2019S LRRK2 were transiently transfected with a plasmid encoding HA-PPM1H. Cells were treated for 30 min with DMSO or SAR405 (3 μM) before immunostaining for HA tag and quantifying the percent of untransfected or PPM1H-positive cells with LRRK2⁺ endosomes. Statistical significance was calculated via unpaired, two-tailed t test with Bonferroni correction (n = 3 wells, >450 cells per well). **(C)** Stable T-REx HEK293 cells expressing GFP-tagged R1441G LRRK2 were transiently transfected with a plasmid encoding either HA-PPM1H or the

(caption continued from previous page) inactive mutant HA- PPM1H H153D. Cells were treated for 30 min with DMSO or SAR405 (3 μM) before immunostaining for HA tag and quantifying the percent of untransfected or PPM1H-positive cells with LRRK2$^+$ endosomes. Statistical significance was calculated via one-way ANOVA followed by Dunnett's post hoc test (n = 3 wells, >300 cells per well). **(D)** Quantification of LRRK2$^+$ endosomes in stable T-REx HEK293 cells expressing GFP-tagged LRRK2 variants treated with SAR405 (3 μM) and monitored via live imaging. After 30 min, DMSO or MLi-2 (1 μM) was added to the cell media. Cells were imaged approximately every 5 min. Data for R1441G is the same as in Fig. 5D. Shaded areas: mean +/- SEM (n = 7 fields of view per condition, >20 cells analyzed per field of view). **(E)** Representative live-cell images of stable T-REx HEK293 cells expressing the indicated GFP-LRRK2 variants after 30 min treatment with DMSO or SAR405 (3 μM). Scale bar, 20 μm. **(F)** Quantification of the percent of cells with LRRK2$^+$ objects observed via live imaging after 30 min DMSO or SAR405 (3 μM) treatment. Statistical significance was calculated via one-way ANOVA followed by Dunnett's post hoc test (n = 6 wells per condition for R1441G LRRK2, 3 wells per condition for other LRRK2 genotypes, >300 cells analyzed per well). **(G)** Scatter plot demonstrating that cellular p-Rab10 levels measured in this work in control DMSO conditions correlate with reported cellular p-Rab10 levels in untreated conditions. Cellular p-Rab10 levels on x-axis were quantified as the mean pT73-Rab10 fluorescence intensity per cell via immunofluorescence after 30 min treatment with DMSO (n = 3 independent experiments, >600 cells analyzed per LRRK2 genotype in each experiment). Cellular p-Rab10 levels on y-axis were estimated from Figure 1 of Kalogeropulou et al[4]. **(H)** Scatter plot demonstrating that SAR405 treatment amplifies cellular p-Rab10 levels ~3-fold (slope = 2.8) across the mutations analyzed. Cellular p-Rab10 levels were quantified as the mean pT73-Rab10 fluorescence intensity per cell via immunofluorescence after 30 min treatment with either DMSO or SAR405 (3 μM) (n = 3 independent experiments, >550 cells analyzed per LRRK2 genotype in each experiment). **(I)** Scatter plot showing low correlation between *in vitro* p-Rab8A levels and cellular p-Rab10 levels in untreated conditions. Data points for both axes were estimated from Figures 1 and 4 of Kalogeropulou et al[4]. Error bars: mean +/- SEM. * indicates p values < 0.05; ** indicates p values <0.01; *** indicates p values < 0.001.

Table A.1: Reported effects of LRRK2 mutations on *in vitro* kinase activity, GTPase activity, GTP binding, and pS935 level. Mutant effects on *in vitro* kinase activity, GTPase activity, GTP binding, and pS935 level are reported relative to WT LRRK2. n/a: not available.

Mutation	**Domain**	**Category**[4-7]	***in vitro* kinase activity**[4, 8-10]	**GTPase activity**[7, 11-14]	**GTP binding**[7, 13, 15-17]	**pS935 level**[4, 8, 17]
T1348N	ROC	Hypothesis-testing	n/a	Decrease	Decrease (GTP-binding deficient)	Decrease
D2017A	Kinase	Hypothesis-testing	Decreased (kinase dead)	n/a	No change	No change or decrease
R1398H	ROC	Protective	n/a	Increase	Decrease	No change
N1437H	ROC	Causal	Small decrease	Decrease	Increase	Decrease
R1441C	ROC	Causal	No change	Decrease	Increase	Decrease
R1441G	ROC	Causal	No change or small decrease	Decrease	Increase	Decrease
R1441H	ROC	Causal	No change	Decrease	Increase	Decrease
Y1699C	COR	Causal	No change or increase	Decrease	Increase	Decrease
R1728H	COR	Risk factor	Increase	n/a	No change	No change or small decrease
I2012T	Kinase	Risk factor	Decrease	n/a	No change	No change or small decrease
G2019S	Kinase	Causal	Increase	No change	No change	No change
I2020T	Kinase	Causal	Decrease, no change, or increase	No change	No change or increase	Decrease
T2031S	Kinase	Risk factor	Increase	n/a	No change	No change
G2385R	WD40	Risk factor	Decrease, no change, or increase	n/a	No change	Decrease

References

1. Erb, M.L., and Moore, D.J. (2020). LRRK2 and the Endolysosomal System in Parkinson's Disease. J Park Dis *10*, 1271–1291. https://doi.org/10.3233/jpd-202138.

2. Martinez, H., García, I.A., Sampieri, L., and Alvarez, C. (2016). Spatial-Temporal Study of Rab1b Dynamics and Function at the ER-Golgi Interface. Plos One *11*, e0160838. https://doi.org/10.1371/journal.pone.0160838.

3. Simonsen, A., Lippe, R., Christoforidis, S., Gaullier, J.-M., Brech, A., Callaghan, J., Toh, B.-H., Murphy, C., Zerial, M., and Stenmark, H. (1998). EEA1 links PI(3)K function to Rab5 regulation of endosome fusion. Nature *394*, 494–498. https://doi.org/10.1038/28879.

4. Kalogeropulou, A.F., Purlyte, E., Tonelli, F., Lange, S.M., Wightman, M., Prescott, A.R., Padmanabhan, S., Sammler, E., and Alessi, D.R. (2022). Impact of 100 LRRK2 variants linked to Parkinson's disease on kinase activity and microtubule binding. Biochem J *479*, 1759–1783. https://doi.org/10.1042/bcj20220161.

5. Biskup, S., and West, A.B. (2009). Zeroing in on LRRK2-linked pathogenic mechanisms in Parkinson's disease. Biochimica Et Biophysica Acta Bba - Mol Basis Dis *1792*, 625–633. https://doi.org/10.1016/j.bbadis.2008.09.015.

6. Taylor, M., and Alessi, D.R. (2020). Advances in elucidating the function of leucine-rich repeat protein kinase-2 in normal cells and Parkinson's disease. Curr Opin Cell Biol *63*, 102–113. https://doi.org/10.1016/j.ceb.2020.01.001.

7. Nixon-Abell, J., Berwick, D.C., Grannó, S., Spain, V.A., Blackstone, C., and Harvey, K. (2016). Protective LRRK2 R1398H Variant Enhances GTPase and Wnt Signaling Activity. Front Mol Neurosci *9*, 18. https://doi.org/10.3389/fnmol.2016.00018.

8. Nichols, R.J., Dzamko, N., Morrice, N.A., Campbell, D.G., Deak, M., Ordureau, A., Macartney, T., Tong, Y., Shen, J., Prescott, A.R., et al. (2010). 14-3-3 binding to LRRK2 is disrupted by multiple Parkinson's disease-associated mutations and regulates cytoplasmic localization. Biochem J *430*, 393–404. https://doi.org/10.1042/bj20100483.

9. Leandrou, E., Markidi, E., Memou, A., Melachroinou, K., Greggio, E., and Rideout, H.J. (2019). Kinase activity of mutant LRRK2 manifests differently in hetero-dimeric vs. homo-dimeric complexes. Biochem J *476*, 559–579. https://doi.org/10.1042/bcj20180589.

10. Jaleel, M., Nichols, R.J., Deak, M., Campbell, D.G., Gillardon, F., Knebel, A., and Alessi, D.R. (2007). LRRK2 phosphorylates moesin at threonine-558: characterization of how Parkinson's disease mutants affect kinase activity. Biochem J *405*, 307–317. https://doi.org/10.1042/bj20070209.

11. Ito, G., Okai, T., Fujino, G., Takeda, K., Ichijo, H., Katada, T., and Iwatsubo, T. (2007). GTP Binding Is Essential to the Protein Kinase Activity of LRRK2, a Causative Gene Product for Familial Parkinson's Disease. Biochemistry-us *46*, 1380–1388. https://doi.org/10.1021/bi061960m.

12. Biosa, A., Trancikova, A., Civiero, L., Glauser, L., Bubacco, L., Greggio, E., and Moore, D.J. (2013). GTPase activity regulates kinase activity and cellular phenotypes of Parkinson's disease-associated LRRK2. Hum Mol Genet *22*, 1140–1156. https://doi.org/10.1093/hmg/dds522.

13. Liao, J., Wu, C.-X., Burlak, C., Zhang, S., Sahm, H., Wang, M., Zhang, Z.-Y., Vogel, K.W., Federici, M., Riddle, S.M., et al. (2014). Parkinson disease-associated mutation R1441H in LRRK2 prolongs the "active state" of its GTPase domain. Proc National Acad Sci *111*, 4055–4060. https://doi.org/10.1073/pnas.1323285111.

14. Lobbestael, E., Baekelandt, V., and Taymans, J.-M. (2012). Phosphorylation of LRRK2: from kinase to substrate. Biochem Soc T *40*, 1102–1110. https://doi.org/10.1042/bst20120128.

15. Ramírez, M.B., Ordóñez, A.J.L., Fdez, E., Madero-Pérez, J., Gonnelli, A., Drouyer, M., Chartier-Harlin, M.-C., Taymans, J.-M., Bubacco, L., Greggio, E., et al. (2017). GTP Binding Regulates Cellular Localization of Parkinson's Disease-associated LRRK2. Hum Mol Genet. https://doi.org/10.1093/hmg/ddx161.

16. West, A.B., Moore, D.J., Choi, C., Andrabi, S.A., Li, X., Dikeman, D., Biskup, S., Zhang, Z., Lim, K.-L., Dawson, V.L., et al. (2007). Parkinson's disease-associated mutations in LRRK2 link enhanced GTP-binding and kinase activities to neuronal toxicity. Hum Mol Genet *16*, 223–232. https://doi.org/10.1093/hmg/ddl471.

17. Purlyte, E., Dhekne, H.S., Sarhan, A.R., Gomez, R., Lis, P., Wightman, M., Martinez, T.N., Tonelli, F., Pfeffer, S.R., and Alessi, D.R. (2018). Rab29 activation of the Parkinson's disease-associated LRRK2 kinase. Embo J *37*, 1–18. https://doi.org/10.15252/embj.201798099.

Publishing Agreement

It is the policy of the University to encourage open access and broad distribution of all theses, dissertations, and manuscripts. The Graduate Division will facilitate the distribution of UCSF theses, dissertations, and manuscripts to the UCSF Library for open access and distribution. UCSF will make such theses, dissertations, and manuscripts accessible to the public and will take reasonable steps to preserve these works in perpetuity.

I hereby grant the non-exclusive, perpetual right to The Regents of the University of California to reproduce, publicly display, distribute, preserve, and publish copies of my thesis, dissertation, or manuscript in any form or media, now existing or later derived, including access online for teaching, research, and public service purposes.

DocuSigned by:
Capria Rinaldi
9382F031751E434...
Author Signature

8/10/2023
Date